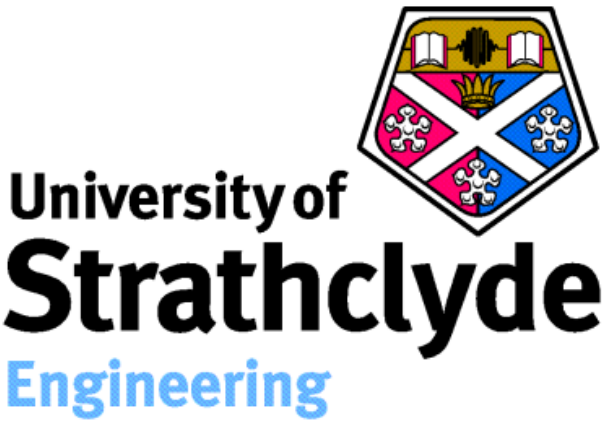

Finite Element Modelling of Healthy and Osteoporotic Bone

Neil James Docherty

The Department of Biomedical Engineering

University of Strathclyde

A thesis presented in fulfilment of the requirements for the degree of MSc.

Supervisors: Dr. Sylvie Coupaud, Dr. Philip Riches

August 2013

Declaration of Authenticity and Authors' Rights

This thesis is the result of the author's original research. It has been composed by the author and has not been previously submitted for examination which has led to award of a degree.

Signed: Date:

Acknowledgements

Many thanks to my project supervisor, Dr. Sylvie Coupaud, for her support and assistance.

I would also like to thank my friends and family, in particular my parents for their continued support throughout the year.

Abstract

Finite Element Modelling of Healthy and Osteoporotic Bone

On a macro-structural level, the bones of the human skeleton is comprised mainly of trabecular (spongy) and cortical bone (dense). Trabecular bone typically occurs at the end points of long bones and has a structure described as a network of plates and rods. Cortical bone forms the hard outer shell and comprised mainly of osteons called Haversian systems. Bone is a composite material consisting mainly of an organic collagenous matrix ad carbonated apatite crystals. The structure of bone material is hierarchically organised and the inhomogeneous nature of bone material results in anisotropic mechanical properties.

Bone adapts to its loading history and undergoes hypertrophy as result of increased loading and atrophy when loading is significantly reduced or completely removed. Osteoporosis is a disease of the bone which is characterised by loss of bone material and hence weakening of the bone. As a result of this, osteoporotic bone is more likely to fracture as a result of everyday loading.

In this study three-dimensional finite element models of the shaft of the tibia were developed using the ABAQUS (Simula) finite element modelling programme. Models were developed to represent three symptoms of osteoporosis – bone thinning, low density and increased porosity. The models were subjected to compressive and torsional loading, and the stress distribution in response to these loads was analysed to gain an understanding of what areas of the tibia are at greatest risk of fracture and under what loading conditions. A risk of fracture for each of the elements was calculated and the maximum risk of fracture in each model gave an indication of fracture likelihood.

This study found that osteoporotic bone showed increased stress and risk of fracture in both compression and torsion. However, torsion of bone with increased porosity was the only combination that produced results that indicate the occurrence of fracture. The aim is for the bone models developed in this study to be used clinically to reduce fracture occurrence in patients with osteoporotic bone loss.

Contents

Chapter 1- Introduction

1.1 Background

1.1.1 Osteoporosis

The bones of the human skeleton are essential for locomotion and for structural support. The ability of the bones to carry out these basic functions becomes compromised in people with osteoporosis. Osteoporosis is a bone disorder which is characterised by high levels of bone loss and diminishing bone mineral density (Ferretti et al, 2003). As a result of these osteoporotic effects, the bone becomes weaker and more susceptible to fracture during everyday activities, thereby severely affecting the structural capabilities of the skeleton. Figure 1 clearly shows how the osteoporotic induced bone loss makes for a more porous and weaker structure.

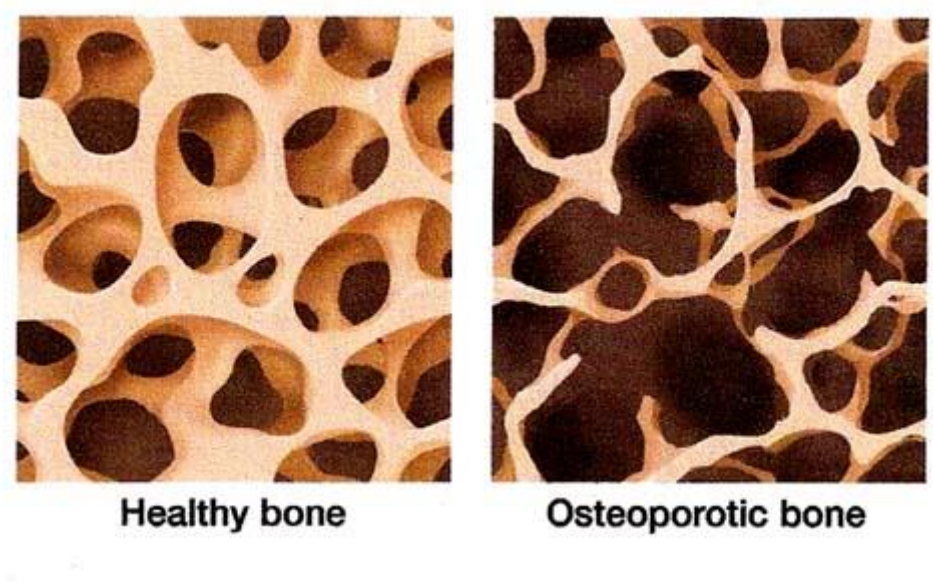

Figure 1: [Comparison of healthy and osteoporotic trabecular bone]
[http://www.drwolgin.com/SiteImages/osteoporosis.jpg]

Osteoporosis is most prevalent in postmenopausal women and the elderly. In the United Kingdom, around 3 million people have been diagnosed with osteoporosis and over 200 million women worldwide are reported to have osteoporosis (Lane, 2006). As the ageing population looks set to further expand and increase, the social

and economic costs of osteoporosis has been predicted to further increase in the future. This suggests that further research into the understanding and prevention of osteoporotic fractures is essential. The fractures that occur due to osteoporosis are commonly known as ‘fragility fractures’ or ‘osteoporotic fractures’ and there are around 3,000 of this type of fracture in the United Kingdom every year (Torgerson, et al., 2001). Due to the elderly population group that the fractures affect, there is a high rate of morbidity and mortality associated with these osteoporotic fractures as compared to fractures of healthy bone. The bone loss and lower bone mineral density that characterises osteoporosis can also be seen in persons with spinal cord injuries (SCI).

Although bone appears to be a fairly inert object, in reality the bones within the skeleton are continually adapting to the loads that they are subjected to. As will be described in more detail, bone atrophy or hypertrophy can occur depending on the bones loading history (Carter, 1984). This type of bone loss observed in SCI persons is referred to as disuse-related bone loss. In SCI persons who rely on a wheelchair for locomotion and support, disuse-related bone atrophy occurs as a result of the skeleton ceasing to be the main structural support for the body and also due to the absence of strain form muscles that have become paralysed (Coupaud et al., 2009). The extensive bone loss that occurs in SCI persons can be related to the level of bone loss observed in extreme cases of osteoporosis. As well as this bone loss, the long bones of SCI persons also show a marked decrease in bone mineral density for a number of year post injury (Coupaud et al., 2009).

1.1.2 Finite Element of Osteoporotic Bone

These characteristic of SCI induced bone loss can be represented in finite element models. Finite element modelling of bone has become increasingly widespread, as it is a technique that allows for the behaviour of bones subjected to *in vivo* loading conditions to be analysed in a safe and effective manner. Accurate representation of bones geometry and material properties allows for this numerical analysis technique to accurately analyse the stress distribution and risk of fracture within healthy and diseased bone.

1.2 Project Aims and Objectives

In this study the finite element modelling package, ABAQUS ®, was used to construct and analyse models of both healthy bone and osteoporotic bone. The aim of the study was to analyse the behaviour of osteoporotic bone under loading and predict which areas are at highest risk of fracture and under what loading conditions.

The constructed finite element models represented the diaphysis of the tibia (the tibia shaft). The load bearing capabilities of the tibia in SCI persons are of particular interest due to the prevalence of tibia fractures within this patient group. Three symptoms of osteoporosis were modelled in this study – bone thinning, low density bone and increased porosity. These osteoporotic models were then compared to a control model which was that of a healthy tibia diaphysis. The results obtained from these models of the tibia diaphysis were compared to models of the full tibia that were constructed and tested in a study carried out by Gislason, M. *et al*., (2013).

The overall aim of this study is to develop finite element models of bone that can be used to accurately capture the behaviour of healthy and osteoporotic bone under a number of different *in vivo* loading conditions. The models can be used as a clinical tool in the prevention of fracture as well as planning of rehabilitation for people suffering from severe osteoporosis and SCI patients.

1.3 Adaptive Behaviour of Bone

Bone is a dynamic material that continually adapts its mass, shape and properties throughout the duration of a person's life. The adaptive behaviour of bone was first noted by Galileo when he stated that body weight and activity related to bone size. This statement was the earliest indication of bones adaptive nature, which is effectively described by Wolff's Law;

'Bone of a healthy person or animal will adapt to the loads under which it is placed.' (Wolff, 1891)

Wolff's law describes that increased loading on a specific bone will result in the bone becoming stronger to resist the specific loading condition. On the contrary, bone can become weaker if loading at a certain point is reduced over time, as the stimulus for remodelling is no longer there. This adaption of bone to develop an

optimised skeletal structure occurs in the form of modelling and remodelling. Modelling is when bone progressively alters its form as a reaction to applied loads or physiologic influences (Clarke, 2008). Removal of old bone and formation of new bone is known as remodelling and can result in bone atrophy or hypertrophy. The process of remodelling is continuous throughout a person life, even starting before birth. This renewal is carried out by bone cells and takes place on the bone surfaces; the periosteal and endosteal surfaces mainly. Trabecular bone has a higher level of remodelling activity due to the obvious greater surface to volume ratio of trabecular bone compared to cortical bone (Seeman and Delmas, 2006). It is thought that bone remodelling serves two main functions; conservation of bone mechanical strength and calcium phosphate metabolism (Hill, 1998). In cortical bone, this strength is maintained by a bone turnover rate of 2-3% each year, whereas for trabecular bone this turnover rate is much higher. This would suggest that turnover of trabecular bone has a more significant role in the metabolism of mineral rather than maintenance of mechanical strength.

1.3.1 Remodelling Process

The remodelling process of bone is overseen by a group of bone cells. This group is referred to as the bone remodelling unit and its role is to resorb old bone and form new bone. There are four types of bone cells which contribute to the remodelling process. Osteoblasts are bone cells which are responsible for the formation of new bone material and osteoclasts are the cells which destroy bone. Osteocytes are the endocrine cells of the bone and act as mechanosensors. A further type of bone cell is the bone lining cells.

There are four distinct stages within the remodelling process; activation, resorption, reversal and formation. Before the remodelling process begins, the bone surface is in a resting state and at any point in time, most of the bone surfaces in the body are in this state. The first stage of the process is activation, which begins with the recruitment and stimulation of osteoclast precursors obtained from the circulation. The job of these cells is to expose the mineralised bone surface by removing the bone lining cells of the surface membrane (Roodman, 1999). In the resorption stage the osteoclasts begin to erode the surface of the bone, which results in the formation of

surface cavities which are known as Howship's lacunae lacunae in trabecular bone and Haversian canals in cortical bone (Clarke, 2008). This erosion of surface bone material is achieved by the osteoclasts mobilising the bone mineral by means of lowering the pH at the resorption areas and subsequently digesting the organic bone matrix (Silver et al., 1988). The next stage of the remodelling process is reversal which links bone resorption to bone formation. This is where new bone starts to be recruited. The final stage in the process is formation, in which the osteoblast cells described previously begin to form new bone. Firstly the osteoblasts begin to synthesise a new collagenous matrix and destroy mineralization inhibitors in order to aid the mineralisation of the organic matrix and the subsequent formation of the bone tissue. The osteoblasts within the new matrix then become osteocytes and develop a canalicular network (Burger et al., 2003). A new cortical or trabecular osteon is formed as a result of the bone remodelling cycle.

1.3.2 Remodelling with Age

Each time a remodelling cycle has been completed, a greater amount of old bone is removed than new bone formed. This means that each time the bone matrix is remodelled, bone is lost and the bone structure is weakened (Zebaze et al., 2010). Bone's remodelling activity is affected in both men and women to differing degrees. The most drastic change is seen in perimenopausal and early postmenopausal women, who often experience extreme cortical thinning (Clarke, 2008). This severe thinning is due to the significant increase in remodelling activity coupled with the difference in bone balance on the periosteal and endosteal surfaces. The bone balance on the periosteal surface is of a slightly positive nature, meaning that more bone is formed than is removed. Whereas on the endosteal surfaces the opposite is true, resulting in the marrow space expanding as bone proceeds to thin form the inside outwards with age (Ferretti et al., 2003).

1.3.3 Intracortical Remodelling

Due to the larger surface to volume area of trabecular bone and hence the greater remodelling activity, this type of bone has long been the focus of remodelling research. This research focuses on the effect of trabecular bone weakness, however Zebaze, R. et al. (2010) have recently shown that intracortical remodelling can

significantly weaken cortical bone. Although the dense nature of cortical bone and its low surface to volume ratio means that it is less likely to be remodelled than trabecular bone, it has been discovered that the Haversian and Volkmann's canals within the bone provide surface area for remodelling from within. The intracortical remodelling sites are depicted in Figure 2.

This remodelling of cortical bone from within causes the cortical bone to becomes more porous, resulting in a significant loss in the strength that is usually associated with the dense nature of cortical bone. Zebaze, R. (2010) reported that this intracortical remodelling accounted for around half of all cortical bone loss at peripheral sites. They also conclude that as the intracortical remodelling process goes on, an increasing amount of surface remodelling area becomes available and the level of cortical remodelling overtakes that of trabecular remodelling at peripheral locations. It has been reported by Han, Z. (1997) that the level of intracortical surface remodelling double that observed on trabecular bone surfaces. This research highlights how the adaptive nature of cortical bone can lead to significant decreases in cortical bone strength and increase in cortical bone fracture risk with age.

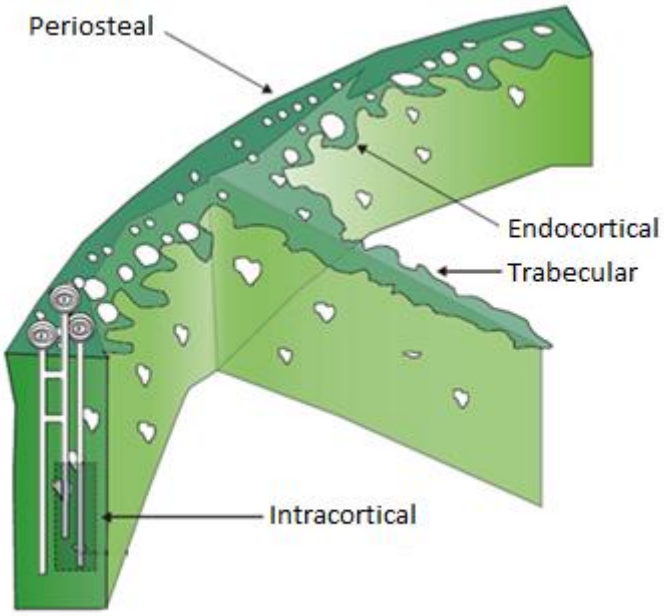

Figure 2: [Location of intracortical remodelling sites, periosteal surface and endosteal surface] [adapted from Zebaze et al, 2010]

1.3.4 Importance of Loading History

The process of remodelling has become fairly well defined over time; however there remains no universal agreement upon the nature of the mechanical stimulant for remodelling. A number of stimulants have been proposed, such as cellular accommodation (Schriefer *et al.*, 2005). However, the most defined mechanical stimulant for remodelling appears to be strain induced by physiological loading. The idea that strains on the bones of the skeleton produced architectural changes to the system was first suggested by Wolff, J. (1891), as stated previously. As early as 1917, a study carried out by Thompson, D'A. (1942) indicated that mechanical deformation caused by loading, resulted in bone remodelling itself in an attempt to resist the specific loading condition that was applied. The mechanostat theory was later developed by Frost, H. (1969) which states that there exists a minimum strain threshold which must be exceeded before bone remodelling can occur. This minimum strain threshold is site specific due to the range of strains that occur at different physiological sites within the skeletal system (Carter, 1984). It is assumed that when the bone is subject to normal loading resulting in strains between 200-2500 microstrains, there is no overall increase in bone formation (Mellon and Tanner, 2012). If a lack of sufficient loading induces strains less than 200 microstrain then the remodelling cycle results in a loss of bone tissue. This strain threshold theory helps explain to some extent, the bone loss that is observed in osteoporosis, spinal cord injury and prolonged periods of space flight. In spinal cord injured patients the muscles become paralysed and no longer exert the same forces upon the bone as they would normally do and the microgravity conditions during space flight significantly reduce the load induced strains on the astronaut's bones. However, there is some argument that this mechanism cannot account for the extreme loss of bone tissue witnessed in patients who have undergone long periods of bed rest (Carter, 1984). On the contrary, when the bone is subject to strains above the upper limit of the strain threshold, osteoblasts are activated resulting in bone formation. The adaption of bone to its loading history as described, illustrates the extent to which a number of factors have upon the health the bones within the human skeleton.

Chapter 2 - Bone Structure and Material Properties

The human skeleton serves a number of both mechanical and metabolic functions. One of the main functions of the bones within the skeleton is to allow for movement and locomotion by acting as levers for the muscles within the body. On a more basic level, the bones of the skeleton also offer protection to marrow and vital organs: the hardness and rigidity of the skull gives the soft tissues of the cranium vital protection during everyday life and the thoracic cavity acts to protect the vital organs within. Bones also serve a metabolic function within the human body which is also essential in preserving quality of life. The bone acts as a reservoir for minerals, in which the majority of the calcium and phosphorus present in the body is stored and distributed when required. A further metabolic function of the skeleton is the maintenance of the acid-balance as a mean's of defence against acidosis (Depts.washington.edu, 1998)

The skeleton is comprised of 213 bones, which can be separated into four distinct categories; long, short, flat and irregular bones (Clarke, 2008). All bone in the skeleton are comprised of dense cortical bone and a porous meshwork of trabecular bone. Long bones consist of a shaft called the diaphysis which is mainly made up of dense cortical bone with an outer periosteal surface and an inner endosteal surface. The metaphysis and epiphysis which are located below and above the growth plates respectively are comprised of trabecular bone encased within an outer shell of cortical bone. The tibia cross section in Figure 3 effectively shows the different bone regions.

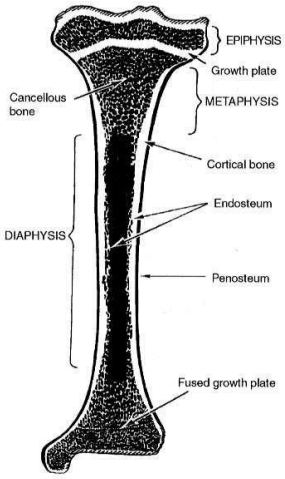

Figure 3: [Structure of a long bone at the macro level] [Dr. Philip Riches. Department of Biomedical Engineering, University of Strathclyde] [Cancellous = Trabecular]

2.1 Hierarchical Structure

In order to understand how the bone as a whole reacts to different loading conditions within the body, it's important to understand the structure of bone and how its components contribute to the heterogeneous and anisotropic nature of the bone material (Pidaparti and Burr, 1992). The structures within the bone material are complex and hierarchically organised (Rho et al. 1998). These structures are specifically designed to optimise bones capability to effectively perform the mechanical and metabolic functions that are essential during everyday life.

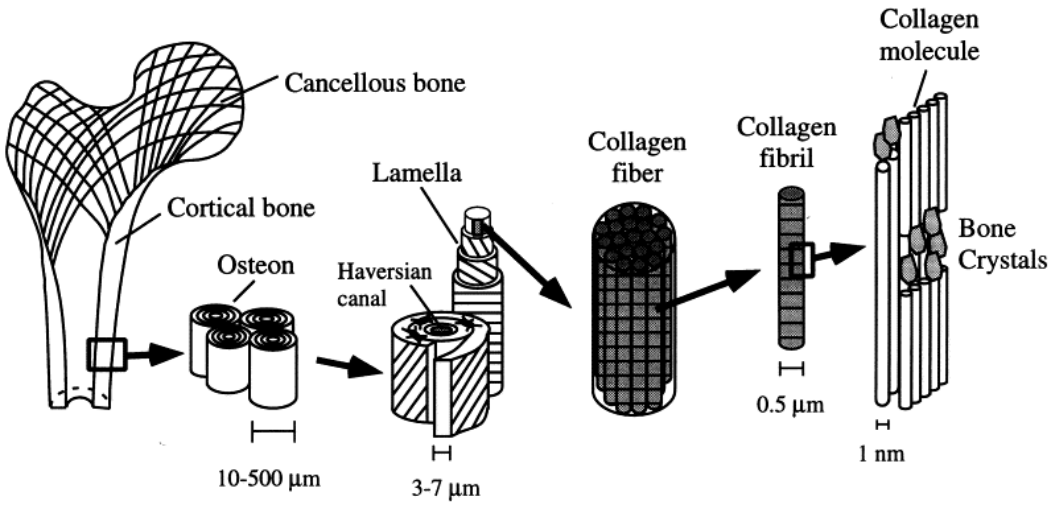

Figure 4: [Hierarchical structure of bone] [Rho et al, 1998]

2.1.1 Nanostructure

In terms of the nanostructure of bone, mineralised collagen fibrils are the basis for all types of bone within the human skeleton. The fibrils form an organic matrix which consists of collagen and non-collagenous organic proteins. This matrix represents around 35% of the bone and the remaining 65% is made up of minerals (Brodsky and Ramshaw, 2004). The fundamental element of the matrix is type 1 collagen molecules, which are secreted by osteoblasts. These type 1 collagen molecules form collagen fibrils in which the mineral crystals are housed. The mineral crystals that transverse the fibrils are predominantly made of carbonated apatite. These apatite crystals are around 2-3 µm thick and are originally needle shaped but become plate shaped as they mature. The way in which the crystals are housed within the collagen fibrils means that initial crystal growth is restricted, resulting in the crystals becoming discrete and discontinuous (Rho, J-Y et al., 1998). There are small amounts non-collagenous proteins present in the matrix and it is suggested by Rho, et al. (1998) that they govern the size and orientation of the mineral crystals. The collagen and mineral composition plays a major role in the mechanical behaviour of bone tissue; this will be discussed in more detail. These collagen fibrils arrange themselves longitudinally to form collagen fibres

2.1.2 Microstructure

The mineralised collagen fibres present in the bone of the developing embryo and infants, form what is known as woven bone. This relatively weak type of bone is comprised of randomly organised collagen fibres in which osteocytes have no specific order. At around two to three years of age, the woven bone present in the long bones is fully replaced with lamellar bone (Cowin, 2001). Lamellar bone consists of arrangements or sheets of mineralised collagen fibres that are constructed to form organised structures called lamellae (Mellon and Tanner, 2012). Lamellae are normally around 3-7 µm in thickness and can form into concentric layers that wrap around a central canal to form osteons which are around 200-250 µm in diameter (Rho, et al. 1998). The mineralised fibres in each lamella of an osteon have differing orientations to maximise the strength of the bone tissue. Cowin, S (2001) describes the orientations of the collagen fibrils within adjacent lamella to be either longitudinal, where they are aligned with the long axis of the lamella or transverse,

where they are perpendicular to this axis. These osteons are present in both cortical and trabecular bone. In contrast to the random distribution of osteocytes within woven bone tissue, ellipsoidal voids known as lacuna host the osteocytes within lamellar bone. As well as forming osteons, lamellae can also occur in stacked layers which are positioned tangentially to the outer surface of the bone. This stacked arrangement of lamellae wrap round the full bone circumference.

2.1.3 Macrostructure

At the macrostructure level, bone tissue can be split into two distinct types; cortical and trabecular. Cortical and trabecular bone are easily distinguishable on the basis of their highly different levels of porosity (Cowin, 2001), however it is important to investigate the differences in bone tissue structure in order to understand how these two types of bone behave under physiological loading conditions. Cortical bone is mainly comprised of osteons which are referred to as Haversian systems, where blood vessels are housed within the Haversian and Volkmann's canals as depicted in Figure 5.

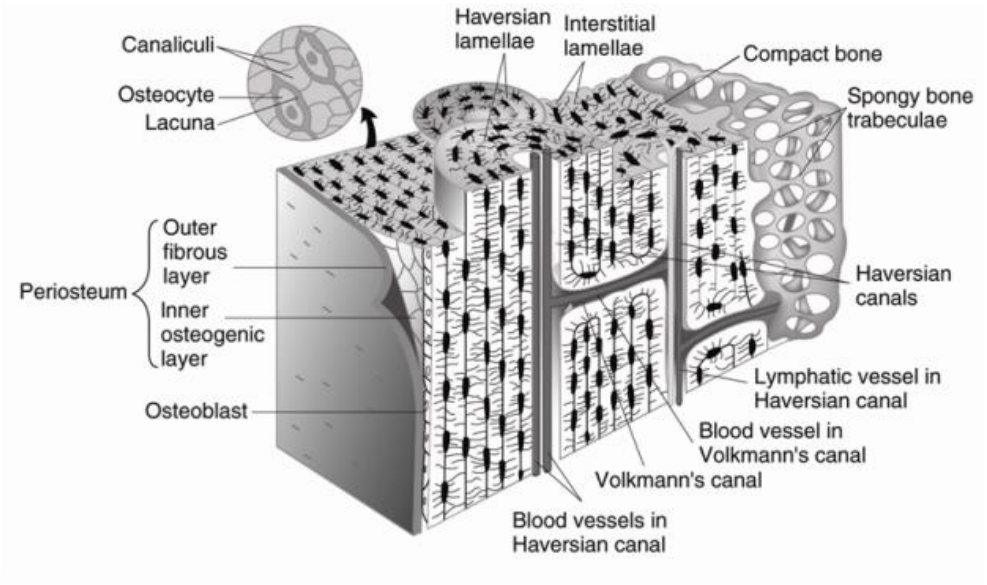

Figure 5: [Internal structure of cortical bone] [http://www.naturalheightgrowth.com]

The Haversian systems are cylindrical in shape and are surrounded by interstitial lamellae within the cortical bone. Less mineralised, collagen rich structures known as

cement lines separate the osteons from the surrounding interstitial lamellae. This arrangement of Haversian systems, interstitial lamellae and cement lines results in the creation of a highly dense material with a porosity of less than 5%. The osteons that are present within trabecular bone tissue are also comprised of concentric lamellae; however, they have a semilunar shape (Clarke, 2008). These trabecular osteons are referred to as packets. The packets form bone tissue in the shape of rods and plates which can be between 50 µm and 300 µm long. These rods and plates are less organised than the osteons within cortical bone however; their alignment is optimised at areas of the bone where physiological loading is high. This combination of bony struts and marrow filled spaces makes trabecular bone a highly porous structure as can be seen in Figure 6.

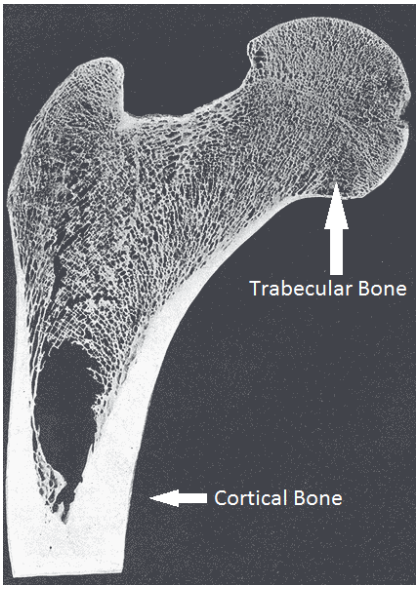

Figure 6: [Locations of Cortical and Trabecular Bone in the Upper Section of the Femur] [http://www.intechopen.com/source/html/42812/media/image5_w.jpg]

2.2 Cortical Bone Properties

In order for bone to function efficiently within the human body, it's vital that bone as a material has the rigidity and ductility required for load bearing as well as the lightness essential for effective locomotion. In this section bone tissue will be analysed as a composite material comprising of stiff carbonated apatite mineral crystals located within a matrix of collagen fibres (Toshiya et al., 2004). The mineral/collagen balance and orientation dictates the mechanical properties of the

bone tissue (Cowin, 2001). The mineral crystals have been shown to possess a high level of stiffness, resulting in a great mechanical rigidity and load bearing strength (Cowin, 2001). In contrast, the post yield ductility is directly related to the collagen fibres within the matrix. The anisotropic form of the mineral crystals results in anisotropic mechanical properties of bone. Bone tissue exhibits elastic, plastic and viscoelastic behaviour in order to effectively manage the different stresses that occur in everyday life.

The structural organisation, the mineral content and the porosity all impact upon the mechanical properties of cortical bone (Clarke, 2008). There have been numerous studies on the mechanical behaviour of cortical bone and although cortical bone is a reasonably uniform structure, many of the results obtained for cortical bone mechanical properties vary significantly. This said to be due to an absence of common experimental methods and objectives as opposed to any fundamental uncertainties. The most widely used techniques for obtaining the mechanical properties of cortical bone are uniaxial tension, uniaxial compression, three/four point bending and ultrasonic velocity tests.

2.2.1 Elastic Behaviour

The term ‘elastic’ refers to mechanical behaviour in which a specimen deforms under an applied stress and then returns to its original form once the stress has been removed. Elastic constants such as Young’s modulus and Poisson’s ratio are commonly used to quantify this relationship between stress and strain in a given material. In general these two constants can be used to describe the basic elastic behaviour of cortical bone under a given loading condition.

The first of the two elastic constants mentioned, Young’s modulus, is used to define the stiffness of the material. This is the value of the stress strain ratio for when the material undergoes a uniaxial tension or compression and is obtained by measuring the gradient of the linear section of the stress/strain curve. Due to the anisotropic nature of cortical bone, the Young’s modulus value varies depending on which direction the specimen is cut. Dempster, W. and Liddicoat, R. (1952) carried out tests on small cubes of human bone in order to determine the Young’s modulus of the specimen in 3 directions; longitudinal, transverse and radial. They observed no

significant difference in the transverse and radial direction with both of these directions having a Young's modulus of around 4GPa. However, they observed a far greater longitudinal Young's Modulus value of 14.1GPa. This study illustrates the anisotropic nature Young's modulus of cortical bone; however, issues with their experimental procedure resulted in fairly low values. Figure 7 shows the longitudinal and transverse stress strain curves for cortical bone which has been tested in tension.

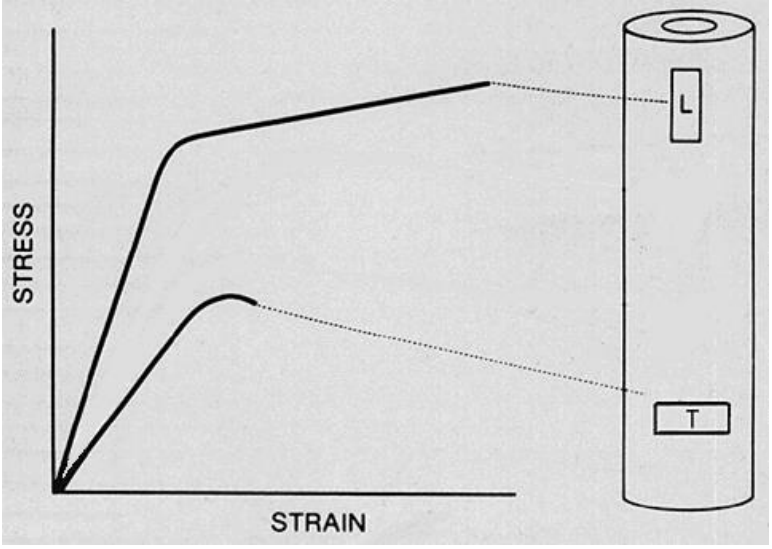

Figure 7: [Stress-strain curves for cortical bone cut longitudinally and transversely] [adapted from http://cal.vet.upenn.edu/projects/saortho/chapter_12/12F8.jpg]

A study carried out by Burstein, A et al., (1973) used a more accurate method in which a clip on strain gauge extensometer was used to measure the bones stiffness within 'physiological' strain rate limits, in order to obtain realistic and useable Young's moduli. They measured the longitudinal Young's modulus to be 17.2GPa and the transverse or radial modulus to be 11.1GPa. These results are more in keeping with other studies in which the transverse or radial modulus is around 14GPa and the Longitudinal Young's modulus is between 17-22GPa (Rho, 1993). It is generally accepted that there is no significant difference between the Young's modulus in compression and in tension (Reilly and Burnstein, 1974). As mentioned previously, the mineral crystals within the bone material have a high level of stiffness, so it would be expected that the level of mineralisation within the cortical bone would have an effect on the Young's modulus. Although the mineralisation

level in bones does not vary greatly, it has been established that a higher level of mineralisation within bone matrix results in an increase in the Young's Modulus and hence a stiffer material (Currey 1988). The review article by Reilly, D. and Burstein, A. (1974) conclude a transversely isotropic material with five elastic constant represents it the elastic behaviour of cortical bone most accurately.

The Poisson's ratio is the negative ratio of transverse to axial strain (Reilly and Burstein, 1974). This governs to what level the specimen is able to bulge under compressive loads or depress inwards when subject to a tensile load. The value of Poisson's ratio for cortical bone is normally around 0.3. However, there is a fairly large range of values throughout the literature. Studies by Lang, S. (1970) and McElhaney, JH. (1965) used the ultrasonic technique and compressive loading respectively, which determined the poisons ratio to be between 0.28 and 0.48 for cortical bone. This value of around 0.3 for cortical bone can be compared to 0.1 of concrete and the maximum possible Poisson's ratio of 0.5 for rubber.

2.2.2 Plastic Behaviour

When a stress is applied to a specimen and it subsequently deforms without returning to its original state once the load in released, this is known as plastic behaviour. It is generally accepted that bone has a plastic region, however, number of studies have shown bone to exhibit different levels of plastic deformation. Dempster, W. and Liddicoat, R. (1952) produced a stress/strain curve for cortical bone in which the curve was a straight line until just prior to fracture, where a small deviation was observed. In contrast, Burstein, A et al. (1973) carried out a longitudinal tension investigation and found that as much as 70% of the total specimen deformation prior to fracture was plastic. There is some discussion about the mechanisms that cause this plastic deformation in cortical bone. It has been suggested that breaking of adjacent molecular bonds on parallel longitudinal planes results in a plastic flow when the bone is subject to tensile loading conditions (Burstein et al., 1973). It's also proposed slip lines occurring within the cortex have a similar effect when the bone is loaded in compression (Chamay, 1970).

2.2.3 Viscoelastic Behaviour

Viscoelastic behaviour is one way a material can deviate from Hooke's law, which states that for a deformation the displacement is directly proportional to the applied force. In a material which exhibits viscoelastic behaviour, the ratio of stress to strain depends upon time or frequency (Cowin, 2001). Viscoelastic behaviour is present in all biological materials and can have a significant effect on the mechanical properties of the material. There are two major viscoelastic processes which contribute to the alteration of bone's mechanical properties. The first is known as creep, where the strain increases with time for a constant stress. Creep studies carried out on cortical bone conclude that bone material shows three stage creep behaviour, as shown in Figure 8.

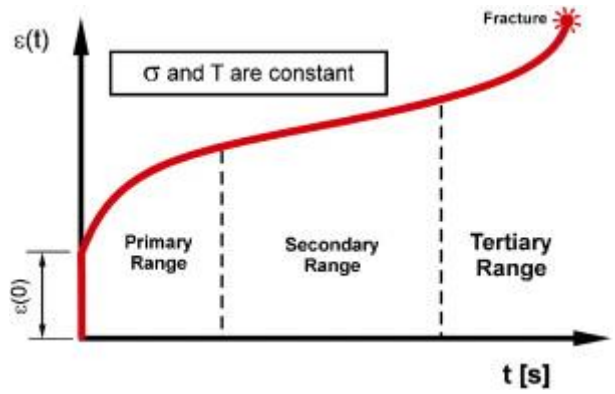

Figure 8: [Classic three-stage creep behaviour shown by cortical bone] [Majda and Skrodzewicz, 2009.]

The initiation of the stress to the bone results in an instant strain increase, followed by the primary stage of creep where the strain follows a rapid downwards concave. The secondary stage of the creep behaviour shows a slower more steady increase in strain over time and the tertiary stage sees the strain follow a faster concave upwards (Cotton et al., 2003). The second viscoelastic process that bone undergoes during loading is stress relaxation (Sasaki et al., 1993). Stress relaxation is defined as a decreasing stress with time for a constant strain. Stress relaxation tests consist of a sudden increase in displacement from zero to a constant level, while the load is measured as a function of time. A relaxation modulus can be used to define the ratio of time dependant stress to strain (Cowin, 2001).

This viscoelastic behaviour that cortical bone shows when loaded, can significantly affect the properties of the bone material. A study carried out by McElhaney, J. and Byars, E. (1965) attempted to quantify the effect of viscoelastic behaviour on the material properties by analysing the reactions of bovine bone to compression testing at varying strain rates. They observed an increase in the value of Young's Modulus and ultimate stress as the strain rate increased. They also noted that with the increasing strain rate, the strain to failure decreased. These results illustrate how this viscoelastic behaviour serves to maintain the rigidly of the skeleton and protect against skeletal damage during loading at high strain rates (Schaffler and Burr, 1988). However, the changes in the material properties of cortical bone resulting from this viscoelastic behaviour are relatively small (Reilly and Burstein, 1974). A number of studies have proven the existence of viscoelastic behaviour in cortical bone, however there is little concluding evidence as to what structures within the bone are responsible for the time-dependent deformation. There is theory that the cement lines located round the edges of the osteons are responsible for the viscoelastic behaviour of cortical bone. This theory is backed up by Lakes, R. and Saha, S. (1979) who subjected bovine cortical bone to prolonged torsional loading and observed displacements located at the cement lines. They claim that these displacements are responsible for the majority deformation over time, and hence a large proportion of the viscoelastic behaviour of cortical bone. The collagen fibres of the bone matrix are said to be viscoelastic in nature, and the carbonated apatite crystals are elastic (Toshiya et al., 2004). As the cement lines appear to be less highly mineralised and richer in collagen, it would be reasonable to expect that they would be a major contributor to the viscoelastic behaviour cortical bone material exhibits. It should be noted that a general agreement on the composition of the cement lines has yet to be reached, meaning it is difficult to conclusively confirm this theory.

2.2.4 Strength

The strength of cortical bone is paramount importance as it dictates what levels of load the bone can endure without fracture. The yield strength of cortical bone is the stress value at which the bone ceases to behave elastically, with plastic deformation occurring after this point. The ultimate strength of the cortical bone material is defined as the maximum stress that the bone sample can sustain under a specific

loading condition without fracture. There are three main testing methods that are used to define the ultimate strength of cortical bone material; uniaxial tension, uniaxial compression and bending tests. The uniaxial tensile tension testing configuration is the most common and reliable way in which to calculate the ultimate strength of cortical bone material (Reilly and Burstein, 1974) The ultimate tensile strength can be easily measured by dividing the greatest sustained load by the original cross-sectional area of the bone specimen. Uniaxial compression tests can be used to calculate the ultimate compressive strength of a cortical bone specimen. This type of loading configuration is thought to yield less accurate results due to the difficulties associated with eliminating the axial inaccuracies and adverse effects of the testing machine. In the past, bending tests were regularly used to calculate the ultimate strength of cortical bone. For this testing set up, cortical bone material was assumed to be fully elastic, when in reality it has a distinct plastic region. Burnstein, A. et al., (1972) stated that this assumption led to overestimation of the ultimate strength when cortical bone is subject to bending loading.

According to a review study carried out by Beaupied, H. et al. (2007) found the ultimate tensile strength of cortical bone to be around 161MPa and the ultimate strength under torsion to be around 84MPa. Although these values give a general idea of the strength of cortical bone material, it should be noted that there are a number of variables which can affect the values. For example, the ultimate strength of the cortical bone material varies depending on the location from which the testing specimen in obtained from (Evans, 1976). Ko, R. (1953) carried out uniaxial tensile testing on cortical bone specimens obtained from a number of anatomical locations and concluded that the ultimate tensile strength of the radius was around 17 per cent greater than that recorded for the femur. They concluded that the radius had the highest ultimate tensile strength, followed by the fibula and tibia with the femur being the weakest. However, it has been shown that the femur exhibits a greater ultimate compressive strength than the radius, fibula and tibia (Reilly and Burstein, 1974).

The ultimate strength values for both compression and tension are dictated by the structure and physiology of the cortical bone material. It is proposed by Currey, J.

(1959) that the amount of Haversian systems within the cortical bone can affect its ultimate strength. They observed higher ultimate tensile strength values for bone specimens that have less Haversian systems and more laminar bone. The Haversian and Volkmann's canals within the Haversian systems are thought to be the reason for this lower strength, as they don't contain any bone material and are have a lower level of mineralisation (Reilly and Burstein, 1974). The ultimate strength values also show marked anisotropy, with differences in ultimate tensile strength for the longitudinal, transverse and radial directions, with a ratio of 6:2:1 respectively (Fan, 2002) There is a theory that suggests this strength anisotropy is a result of the differing orientations of the collagen fibres (Pidaparti and Burr, 1992). They claimed that a greater tensile strength is observed when there are more longitudinally orientated collagen fibres and conversely, the compressive strength increases with more transversely positioned collagen fibres. This theory that collagen fibre orientation is the reason for the anisotropic strength of has been the topic of a number studies (Reilly and Burstein, 1974; Evans and Vincentelli, 1969). However, there remains an absence of conclusive evidence that this tissue strength anisotropy is solely due to the collagen fibre orientations.

The level of mineralisation within the bone material is also a major determinant of its ultimate strength. It is generally accepted that a greater level of mineralisation leads to a greater ultimate strength. At the osteon level, fully mineralised osteons show a 20 per cent higher ultimate tensile strength and a 70 per cent larger ultimate compressive strength in comparison to initially calcified osteons produced during the remodelling cycle (Reilly and Burstein, 1974). This relationship of increased ultimate strength with increasing mineralisation was also found to be true at the structural level of cortical bone when a bending load was applied (Currey, 1969). As well the mineralisation level having an effect upon the strength of the bone, an increased level of porosity resulting from age or disease also decreases the strength of the cortical bone.

2.3 Trabecular Bone Properties

The mechanical properties of trabecular bone are also of great interest, due to the increasing prevalence of age- related fractures at sites comprised mainly of trabecular

bone. As a result of the complex and porous structure of trabecular bone, it is difficult to obtain an accurate representation of the elastic, plastic and viscoelastic behaviour of trabecular bone (Cowin, 2001). There are a number of both experimental and theoretical techniques which are widely used in an attempt to gain the most reliable mechanical properties for trabecular bone. The most common type of mechanical testing that is carried out on trabecular bone specimens in uniaxial compression, when the modulus is calculated from the incurred displacements. The Young's Modulus values in the literature vary considerably and recent investigations have shown that this could be partly due to some inherent errors with the uniaxial compression testing method. Frictional end effects during compression of the trabecular bone specimen can lead to over estimation of the modulus whereas underestimation of the modulus occurs as a result of damage to the bone tissue as the specimen is machined to shape (Keaveny and Hayes, 1993). Recently an ultrasonic wave method has been used in order to eliminate the errors associated with uniaxial compression testing. This ultrasonic wave method calculates the Young's modulus using the measured velocity of the ultrasonic waves as they move through the specimen and the apparent density of the bone specimen (Ashman and Rho, 1988). A major advantage of this technique is that the anisotropic nature of the mechanical properties can be captured, as the Young's modulus can be measured in all three orthogonal directions. However, the ultrasonic wave technique does not allow for the viscoelastic properties to be measured. Bucking tests are also used to investigate the mechanical properties of trabecular bone as this is a common failure mode of trabecular bone when loaded in vivo. Within the literature, there isn't the abundance of tensile data for trabecular bone as is that is available for cortical bone. This is partly due to difficulties in obtaining specimens long enough to undergo tensile testing.

Quantitative Commuted Tomography (QCT) has been used as a non-invasive method of measuring the mechanical properties of trabecular bone. This technique allows for the apparent density of the trabecular bone to be calculated, as this is linearly related to the QCT-density. Form this apparent density value obtained, the Young's modulus and strength can be easily calculated (Keaveny and Hayes, 1993). This method has

become increasingly popular due to its non-invasive nature and the ease at which a number of anatomical sites can be scanned

2.3.1 Elastic Behaviour

Across the literature on trabecular bone, there is a large variation in its elastic properties, in particular for the Young's modulus. A buckling experiment carried out by Townsend, P. et al. (1975) on human trabecular bone tissue obtained from the proximal tibia calculated the Young's modulus to be 11.4GPa. This is a fairly typical value, however there is wide range of values found within the literature; the Young's modulus values for trabecular bone range from 1-13GPa (Keaveny and Hayes, 1993). This wide range of values underlines the uncertainty that remains as to what values give a true representation of trabecular bone stiffness. Despite this ambiguity, the Young's modulus of trabecular bone is generally considered to be approximately 20-30 per cent less than that of cortical bone (Choi and Goldstein, 1992). This difference can be attributed the differing levels of mineralisation and to the structural differences between trabecular and cortical bone at the micro and macro level (Choi et al., 1990)

There are a number of variables which can affect the stiffness values obtained for trabecular bone material. The heterogeneity of trabecular bone means that the Young's modulus varies greatly for specimens of bone taken from different anatomical locations and even for specimens taken from the same metaphysis (Goldstein et al., 1983). The porous structure of rods and plates that trabecular bone exhibits means that its elastic properties also show anisotropy; the Young's modulus value is dependent upon the direction of loading. Age is a further variable which has an effect on the stiffness of trabecular bone. A study carried out by Mosekilde, L. and Danielsen, C. (1987) concluded that the Young's modulus decreased by around 17 per cent with each decade of life. Due to these afore mentioned variables and the effect of disease, the true value for Young's modulus should be defined taking into account the effect of all of these variable for each individual case. With regards to the Poison's ratio of the trabecular bone tissue, it has been measured to be anything from around zero to 0.5, so it is generally assumed to be 0.3 for experimental testing purposes (Keaveny and Hayes, 1993)

2.3.2 Plastic Behaviour

In a similar fashion to cortical bone, trabecular bone also exhibits a distinct plastic region after a short period of period of elastic behaviour. Once the yield point has been reached, strains occur that result in a negligible change in stress. This is followed by a further region of stiffness as shown in the graph in Figure 9. Buckling and collapse of the rods and plates within the trabecular bone are accountable for this region immediately after the yield point. Once these rods and plates have completely collapsed then the trabecular bone is compact, hence the observed region of stiffness.

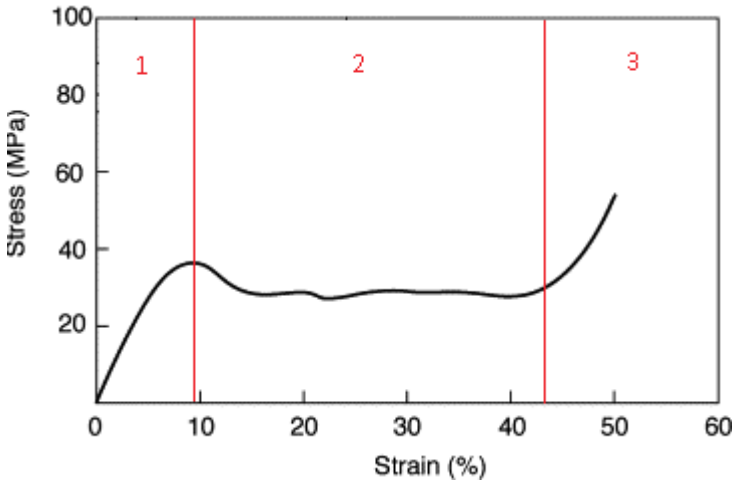

Figure 9: [Stress-strain response of trabecular bone loaded in compression. Region 1 represents the elastic phase; region 2 begins at the yield point and represents the period of plastic deformation; region 3 represents the second phase of stiff behaviour] [Adapted from Mercer et al., 2006]

2.3.3 Viscoelastic Behaviour

There is also a noted viscoelastic response to loading by trabecular bone, showing marked stress relaxation and creep. (Linde et al., 1991) carried out a study in which specimens of trabecular bone were compressed uniaxially at different strain rates, in order to determine the time-dependent properties of the tissue. They observed a greater strength and stiffness as the strain rates were increased, a theory which generally agreed upon (Carter and Hayes, 1977) It has been suggested that the marrow that fills the spaces within the plates and rods of trabecular bone, can have a stiffening hydraulic effect at high strain rates during experimental testing and standard strain rates when in vivo (Keaveny and Hayes, 1993).There has been little conclusive research into the stress relaxation and creep observed in trabecular bone.

The studies that have focused on this aspect of viscoelastic behaviour, propose that trabecular bone shows the same three stage creep as is shown to be the case for cortical bone previously (Cotton et al., 2003).

2.4 Bone Fractures

As previously stated bone is responsible for maintaining the body's structure and bearing everyday forces and loads. Fracture to the bone can greatly compromise its ability to perform these vital functions. This section will investigate the mechanics of fracture and the relationship between bone mineral density and risk of fracture.

2.4.1 Fracture Mechanisms

It is generally accepted that the event of bone fracture occurs when a critical strain is reached. This implies that when a bone is loaded, fracture occurs at the point when maximum strain is applied and not the point of maximum stress (Ritchie et al., 2006). The characteristics and mode of fracture differ, depending upon the direction and type of loading the bone is subject to. When a tensile load is applied to the bone in a direction parallel to its long axis, the fracture orientation is approximately 45 degrees to the line of the applied tensile load (Wang et al., 1998). This infers that the tensile loading of the bone also has a shear element. The failure under this loading condition can be attributed to tearing of the fibres within the organic bone matrix, cracking and creation of slip lines. When bone is subject to compressive loading along the same axis, the fracture occurs due to microbuckling. This mocrobuckling mode of failure is when the inner structures of the bone become unsteady and kinking or bowing results as a consequence. Due to the heterogeneous nature of bone tissue, the compressive force results in shear stresses between the components of the bone which have differing mechanical properties (Rho et al., 1998). When a force perpendicular to the bones long axis is applied with sufficient magnitude to produce fracture, this fracture occurs by means of a simple sharp division of the bone. The line of the fracture propagates though the cement lines located round the osteons within the bone. This means that in cortical bone the fracture line seldom splits an osteons, meaning that the Haversian canals remain intact. The fracture line also follows a similar bath when the bone is subjected to bending leaving the Haversian

systems fairly unharmed. Piekarski, K. (1970) carried analysis on the characteristics of fractures due to bending of a cortical bone specimen and observed that full osteons were ripped out and the crack moved through the cement lines. This behaviour observed during perpendicular loading, torsion and bending reinforces the theory that, within bone tissue the cement lines the weakest structure (Ritchie et al., 2006). The crack produced by a torsional loading induced fracture scenario follows a helical path and begins with a distinct shear step.

2.4.2 Fracture Propagation Resistance

After the event of fracture has occurred, the bone material employs toughening mechanisms in order to limit the damage incurred as a result of the crack. There are two categories of toughening mechanism that control the propagation of a crack. The first types are intrinsic mechanisms which act in front of the crack tip. The second class of toughening mechanisms are extrinsic mechanisms which act away from the tip of the crack. This type of mechanism attempts to protect the bone by reducing the magnitude of the applied force as it moves through the crack. The main way in which the driving force is buffered is by crack bridging, in which un-cracked ligaments or single collagen fibrils span the crack away from the tip to reduce the intensity of the stress that is experienced at the crack tip (Nalla et al., 2003). Other extrinsic mechanisms include the deflection of the crack by osteons and the formation of microcracks around the main crack which act to compress the crack tip in an attempt to slow its propagation. It's proposed that effectiveness of these toughening mechanisms diminishes with age, meaning that fractures in older people cannot be managed and are able to become more destructive to the bone tissue.

2.4.3 Bone Mineral Density and Fracture Risk

Bone mineral density is the mineral matter per square centimetre of bone tissue and is closely linked to the apparent bone density. Low bone density is a fundamental symptom of osteoporosis and the measurement of the bone density is widely used as a way to establish the bone risk of fracture. As described previously, the increased rate of remodelling witnessed in osteoporotic bone results in a net loss of bone. The bone that is formed is less highly mineralised and has a significantly lower density than healthy bone. The QCT scan technique for determining bone density mentioned

previously, gives a measure of the bones volumetric density in order to distinguish osteoporotic bone from healthy bone. Bone density is normally expressed in standard deviation units called T-scores. T-scores are developed for comparison of the obtained density values to that of healthy young adult's .A reference T-score value is assigned to the associated bone density value of the young healthy individual. Bone can be categorised as osteoporotic if the bone density value is 2.5 standard deviations or more below the reference value (WHO, 2004). This bone density based method of diagnosing osteoporosis is now common clinical practise. In postmenopausal women the occurrence of fracture increases with decreasing levels of bone density (Mcclung, 2005). Although the general acceptance is that low levels of bone density lead to an increased likelihood of fracture, it should be noted that there are other factors that should be taken into account.

Chapter 3 - Finite Element Modelling

Finite element modelling (FEM) is the process by which a computer model of an object or material is created and subjected to specific loading stresses which subsequently produces values for analysis. This is an analysis technique which uses numerical analysis in order to calculate approximate solutions for a range of different types of loading scenarios, which can be used to predict how the object will behave in the real world. These solutions can be in the form of heat flux, mechanical stress, electric field, magnetic field and fluid velocity. The finite element method has been commonly used in industry in some form since around the 1950'sand is now being used to analyse the behaviour of biological tissues and in particular, bone.

3.1 Finite Element Method

3.1.1 Method

All types of finite element modelling and analysis begin with the definition of the object or objects geometry. True representation of objects real world geometry can be easily obtained by using the sketch function to create the basic shape and dimensions. The object can be further refined using extrude, revolve, sweep etc. functions to achieve the desired part geometry however complex it may be. Once the geometry of the part has been accurately created, a process of meshing, also known as discretising is carried out. This is where the part is split into finite elements which are joined together by a number of nodes. These two-dimensional or three-dimensional finite elements come in a number of different shapes and sizes, depending on the geometry of the part that the mesh is assigned to. For example there are a number of differently shaped continuum elements, shell elements, truss elements, beam elements etc. Figure 10 shows a basic hollow cylindrical part which has been assigned a mesh consisting of hexahedral shaped continuum elements.

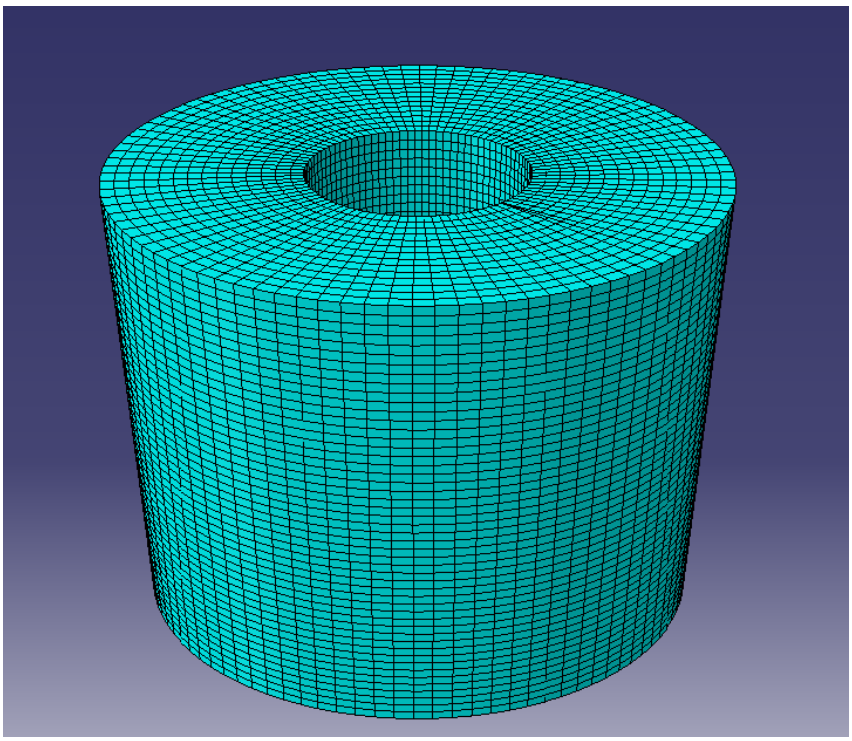

Figure 10: [Cylindrical model discretised with eight-node hexahedral continuum elements]

Each of the finite elements represents a distinct segment of the overall part, and the amount of elements that are present per unit length or volume is known as the mesh density. The results of the finite element analysis become increasingly more accurate with increasing mesh density. However increasing the mesh density also results in a longer computing time when running the analysis. The nodes of each finite element also vary in number. The nodal displacements are the fundamental basis for the calculation of the solutions in finite element analysis. The part is assigned specific material properties according to the object or material it is representing. Before the loading conditions are applied to the discretised part, boundary conditions must be defined. These are the applied constraints that govern the models movement in space, as they dictate what degrees of freedom are active the geometry, nodes or element. The model is then subject to a specific loading condition and the results can be visualised by means of a contour on the deformed model and analysed though numerical solutions and graphical representation. The results of a finite element analysis can be compared to those obtained experimentally to validate the finite element model.

3.2 Finite Element Modelling of Bone

Finite element modelling of bone has become an increasingly popular and effective way to capture the in vivo response of bone to a variety of situations and loading conditions. Three dimensional models of whole bones are regularly constructed in order to analyse the bones behaviour to different physiological loading scenarios and how the response is altered due to disease. It is now possible for patient specific three dimensional bone models to be constructed which will be described in detail later in this chapter. These bone models can also be used to test implants in a clinical setting. This section of the study will focus on the construction and analysis of three-dimensional finite element modelling of the bones in the lower leg. A large number studies have applied the finite element method to model the bones of the lower leg and this chapter will evaluate the accuracy and reliability of FE modelling of bone. The accuracy and reliability of finite element bone models depend upon the creation of realistic geometry, material properties and boundary conditions.

3.2.1 Construction of FE Model

Finite element studies of bone generally construct models of the whole bone or small sections of cortical or trabecular bone. The construction of segments of cortical bone material is achieved by simply modelling the desired shape of the specimen using the geometry tools within the finite element programme. Larger scale models of bone can also be constructed this way, however the simple nature of the shape as compared to that of the real bone means that a number of assumptions have to be made and the results of the analysis may be slightly less accurate. In order to achieve a more realistic representation of the bones behaviour on a global scale, patient-specific bone models can be created using data from quantitative computed tomography (QCT) scans. These QCT derived bone models are of great clinical use as they are patient specific and capture the combined response of the trabecular and cortical bone to various loading conditions. Recent advancements in QCT and finite element methods have allowed for this method of deriving patient specific and highly accurate bone models, and has become increasing popular for both experimental and clinical use. In order to obtain the geometry of the bone, the coordinates of the

individual voxels obtained from the QCT scan are used. Figure 11 shows the discretised femur models created using data obtained from a QCT scan.

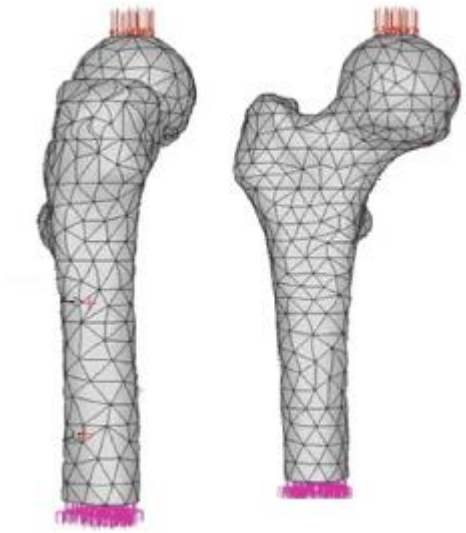

Figure 11: [QCT derived models of the human femur discretised with tetrahedral elements.] [Yoshibash et al., 2007]

The density of each voxel can be established by its gray level intensity. This density obtained from QCT scan images is measured in Hounsfield units which can be correlated to find the Young's modulus. There still remains the relative ambiguity of distinguishing between the cortical and trabecular bone due to the absence of an exact cut off density value for each bone type. However a number of studies have set a precedent for this determination of cortical and trabecular bone. It is generally considered that apparent bone density values obtained from QCT that are less than $0.7 g/cm^3$ can be classed as trabecular bone and values greater than this are regarded as cortical bone. Around $1.2 g/cm^3$ is considered to be the average density value of healthy cortical bone. The mechanical properties of the cortical and trabecular parts of the model can be calculated either by finding an average density value for the full bone and subsequently calculating the Young's modulus from this or by computing the Young's modulus for each individual voxel and assigning the average Young's modulus to the model.

It important that the correct type and size of element is used to discretise the bone models in order to gain an accurate representation of the stress distributions and other

results throughout the non-uniform geometry of the bones in the lower leg. In general, three-dimensional tetrahedral or hexahedral elements are used to model the femur, fibula and tibia. A study carried out by Yoshibash, Z. *et al*. (2007) developed isotropic inhomogeneous QCT scan derived models of the femur and discretized one with hexahedral elements and the other with tetrahedral elements. Two loading conditions were applied to the models in order to analyse the effectiveness of these element types; a pressure load was applied to the femur head. The two mesh types were slightly altered in order obtain an optimum polynomial degree shape function and the energy values were compared to that of experimental results to establish the degree of error present in each model. For the femur model that was discretised with optimised tetrahedral elements the error was less than two per cent and for the optimised hexahedral element model the error was less than 6 per cent. The results that were obtained for both types of element indicated that the displacement and stress values were similar to those that have been experimentally calculated for the same loading conditions (Yoshibash *et al.,* 2007). The results of this particular study imply that the use of hexahedral or tetrahedral is appropriate when constructing finite element models of the long bones. As mentioned previously, the size of the elements that are used is as important as the type. A study carried out by Keyak, J. and Skinner, H. (1992) constructed models of the femur and assigned element sizes of 3.1mm, 3.8mm and 4.8mm. They found that when the models were loaded and analysed, the stress vales that were calculated decreased with increasing element size. An increase in element size from 3.1mm to 3.8mm resulted in a 16 per cent difference in the stress values. It's recommended that when constructing finite element models of bone, the element size must be less than 3mm to accurately capture the bones complex mechanical properties (Kejak and Skinner, 1992).

3.2.2 Material Properties of FE Model

The assignment of realistic material properties to the bone models is one of the most important factors in achieving accurate and reliable results and there is still some uncertainty over what type of material is best suited to finite element bone models (Baca *et al.,* 2008). As previously described in Chapter 2, both cortical and trabecular bone are composite materials with anisotropic and inhomogeneous mechanical properties which are difficult to accurately represent within a finite element model.

For this reason, a number of studies have assigned isotropic material properties and modelled bone as linear elastic. However, it has been suggested that more accurate and reliable results from finite element bone studies can be obtained by modelling bone as transversely isotropic, hence capturing some of the complexity of bones mechanical properties (Sharma *et al*, 2012). Sharma, N. *et al.* (2012) carried out a study in which specimens of cortical bone where modelled using transversely isotropic material properties and subjected to axial and biaxial loading conditions. The transversely isotropic nature of the cortical bone specimens was achieved by defining five elastic properties. They assigned longitudinal and transverse Young's moduli and shear moduli, as well as a constant Poisson's ratio. The values which were used in this study were experimentally obtained in order to gain the highest possible accuracy when analysing the use transversely isotropic material properties. They analysed the Von Mises stress distribution and anisotropic yield behaviour of these specimens using the finite element analysis programme ABAQUS®. 20 node hexahedral elements were used to discretise the models due to the simple geometry of the bone specimen models. This study concluded that the stress strain values obtained correlated well with the experimental results for the uniaxial tensile and transverse loading. However, they noted that the stress-strain values differed from the experimental results at the instant where the material begins to harden and onwards. Overall this study illustrates that the use of transversely isotropic material properties for cortical bone yields stress values that are close to those obtained experimentally and hence useful for clinical and experimental use.

Several comparison studies have been carried out in order to provide more clarity on the effects of using isotropic homogenous material properties as opposed to material properties which are a truer reflection of bones anisotropy. Barca, V. *et al.* (2008) carried out a study in which the whole femur was modelled and loaded in uniaxial compression. Three whole femur models were constructed from QCT scan data, discretised with 1mm sized tetrahedral elements and each model was given a different set of material properties. The isotropic homogenous model was represented by two elastic constants; this model was assigned a Young's modulus value and a Poisson's ratio. The isotropic inhomogeneous was generated by creating 70 material groups in accordance with the density values obtained for the QCT scan. A third

model of orthotropic inhomogeneous nature was produced by splitting the 70 material grouping into 30 orthotropic directions in order to represent the difference in the bone's material properties in different directions. Again the ABAQUS® software was used to simulate the loading of the femur models and the displacements measured in each model was compared. This study observed that the displacement values for the isotropic homogenous and the orthotropic inhomogeneous model differed by 4.8 per cent, which they considered to be satisfactory for a biological finite element analysis. In general, the use of either an isotropic homogenous set of material properties or transversely isotropic/orthotropic inhomogeneous material properties both result in similar and accurate results for cortical bone models and for whole bone models (Peng *et al.* 2006).

3.2.3 FEM to Simulate Physiological Loading Conditions

It is vital that the loading conditions that bones are subjected to in vivo can be accurately replicated using the finite element method. These in vivo conditions allow for the bone models to be tested in order to determine accurate fracture loads, which would not be possible to do in living subjects. A study carried out by Wong, C. *et al.* (2010) investigated the accuracy of the finite element modelling method for predicting the fracture likelihood and location in the bones of the lower leg (tibia and fibula). Tibia fractures are a relatively common occurrence when the tibia has sustained significant osteoporotic bone loss. This particular study used QCT data to construct a lower leg finite element model consisting of a tibia model and a model of the fibula. These models were assigned a mesh of tetrahedral elements and isotropic homogenous material properties. Three types of loading conditions that can produce a fracture in vivo were applied to the lower leg finite element model. The first loading condition was uniaxial compression. In order to produce a realistic loading scenario, 60 per cent of the 800N load was distributed over the medial side and 40 per cent over the lateral side of the proximal surface of the tibia. The lower section of the tibia and fibula model was fixed in all three orthogonal directions meaning that no translations or rotations could occur at this point. The models were also subjected to a torsional loading condition, in which the proximal and distal sections of the tibia and fibula models were subjected to an external rotation of 1,000N around the longitudinal (Z) axis, applied at the outer edges of the bone A transverse loading

condition was also created by applying bending loads of 5,000N and 2,500N to the nodes on the tibia diaphysis and fibula diaphysis respectively. Fixed rotation/displacement constraints were applied to the proximal and distal ends of the lower leg model in order to recreate typical three point bending conditions. The Von Mises stress values and distribution resulting from the simulation of these three loading conditions was used to analyse the behaviour of the lower leg bones in response to these typical fracture inducing loading conditions. This study also calculated a risk of fracture (RF) value for each of the loading conditions, which would be an effective clinical tool. The value for the RF was derived using the calculated Von Mises stress and the ultimate stress as show in Equation 1.

$$RF = \frac{\sigma_{vm}}{\sigma_{UTS}} \quad (1)$$

This method for estimating a risk of fracture has been used in a number of studies and is derived from a factor of safety (FOS) equation that was developed in a study carried out by Keyak, J. and Skinner, H. (1992), in which femoral fracture loads where estimated using the finite element method. This formula can be seen in Equation 2.

$$FOS = \frac{\sigma_{UTS}}{\sigma_{vm}} \quad (2)$$

They state that for elements with a factor of safety less than one, failure will occur. So when using the RF equation in this study, elements with a RF greater than one can be said to have experienced fracture. The fracture locations and patterns of fracture for each loading condition were considered to be accurate; however the study observed lower RF values than similar experimental studies suggested (Ebacher *et al.*, 2007). The lower RF values that were witnessed could be due to the assumption of isotropic homogenous mechanical properties (Wong et al., 2010). Despite the slightly lower values RF values, the correct calculation of fracture locations and patterns suggest that this sort of lower leg finite element model analysed using Von Mises stress could be used effectively as both an experimental and clinical tool.

3.2.4 FEM of Osteoporotic bone

There has been a number of studies with have used the finite element method to assess the effect of age and disease on bone. A study carried out by Gislason M. et al (2013) specifically analyses the effect that disuse-related bone loss incurred by SCI persons, has on the risk of fracture under physiological loading conditions. They use QCT derived bone models of the tibia which have severely differing levels of density along the length of the bone. Compressive, bending and torsional loads were applied and the risk of fracture equation mentioned in Equation 1 was used to assess what affect the low density of SCI persons bone has on its fracture prevention capabilities. This study illustrates the suitability of the finite element method to effectively capture the effects of disuse-related bone loss.

Chapter 4- Methodology

The finite element modelling and analysis process for this study was carried out using the finite element modelling programme ABAQUS ® /CAE from SIMULA ®. As mentioned in the previous chapter, this modelling programme has been effectively used in a number of finite element studies of bone. This study will focus on the tibia, in particular the diaphysis section as this area of the bone has been proven to be most susceptible to fracture in osteoporotic bone (Gislason et al., 2013). The models that were constructed in this study aim to analyse the response of the cortical bone in the diaphysis to common loading conditions. Models of able bodied bone will be compared to models which represent the common effects of bone loss seen in osteoporosis. The effects of bone loss that will be represented in this study are bone loss from the endosteal surface, increased area of low density bone around the endosteal surface where remodelling rates are high and increased general porosity caused by increased remodelling.

4.1 Model Geometry

There were six geometrically different models that were analysed in this study. The first two models that was subjected to loading conditions and analysed, were segments of the tibia diaphysis around 2cm in length. The geometry of the subsequent four models was more representative of the full diaphysis of healthy and osteoporotic tibia.

4.1.1 Segment of Diaphysis

A section of healthy cortical bone from the diaphysis of the tibia was modelled as a simple hollow cylinder with an outer diameter of 0.03m, an inner diameter of 0.008m and a length of 0.02m. The geometry was then altered to represent the same section of tibia, except with osteoporotic bone loss. This was achieved by increasing the inner diameter to represent loss of bone from the endosteal surface, as this bone is the first to be lost with ageing (Ferretti et al., 2003). The inner diameter of the osteoporotic bone loss model was 0.015m which represented a significant amount of remodelling induced bone loss from the endosteal surface. This loss of bone from the endosteal surface can be clearly seen in the four cross sectional images obtained from QCT scans of an able bodied control and chronic spinal cord injured patient that are

depicted in Figure 12. The areas of light colour represent highly dense cortical bone while the dark areas are the areas of lower density trabecular bone and marrow space.

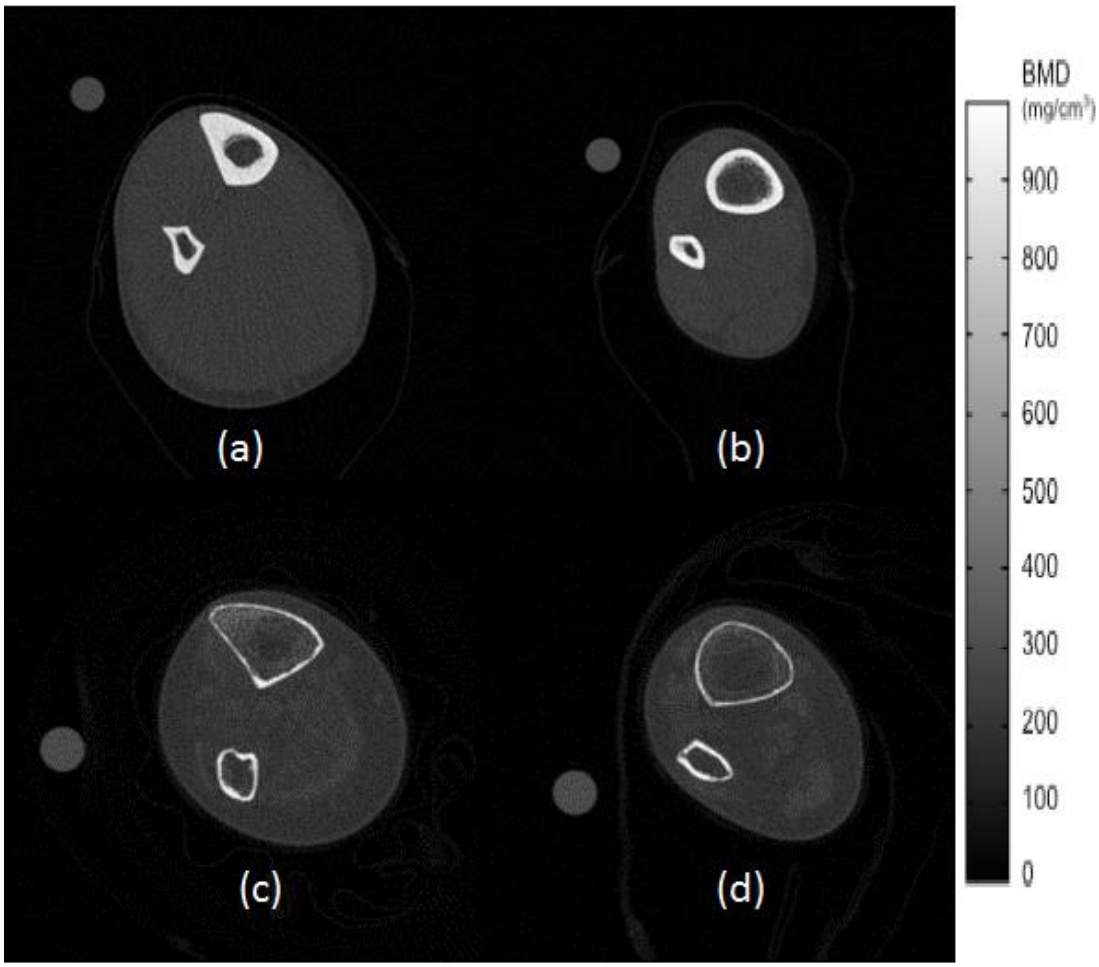

Figure 12: [Four QCT scans of the tibia and fibula of both able bodied controls and chronic SCI patients. a) and b) Scans from the able bodied control showing normal levels of cortical and trabecular bone. c) and d) Scans from a chronic SCI patient showing cortical thinning due to loss of cortical bone from the endosteal surface] [Dr. Sylvie Coupaud. Bioengineering Unit, Strathclyde University]

As these images show, there is substantial loss of cortical bone from the endosteal surface throughout the tibia diaphysis of SCI persons.

4.1.2 Full Diaphysis

The complete healthy diaphysis of the tibia was modelled with simplified geometrical characteristics. Due to the average length of a male tibia being reported as 36.48cm in a study carried out by Hrdlicka, A. (1898), the length of the full diaphysis model was 0.33m with the anterior posterior and lateral diameter of the

tibia shaft being 3.13cm and 2.24cm respectively. These sizes are only approximations due to the large variation in tibia size from person to person and that, although the cross sectional sizes are given as diameters, the tibia is clearly not cylindrical in shape. The tibia cross sectional image obtained from a pQCT scan shown in Figure 13 illustrates that the cross sectional shape of the diaphysis is roughly triangular.

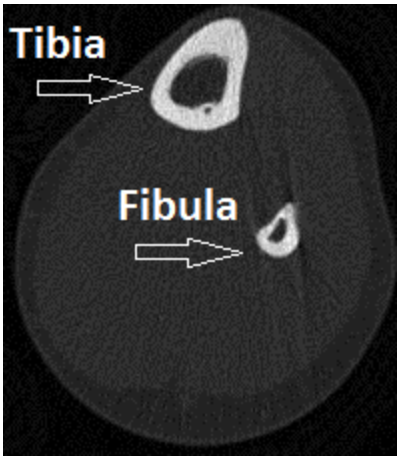

Figure 13: [QCT image of the tibia and fibula representing the triangular like cross-sectional shape] [Dr. Sylvie Coupaud. Bioengineering Unit, Strathclyde University]

This triangular cross sectional shape was represented with a maximum anterior posterior width of 0.033m and a maximum lateral width of 0.025m as depicted in Figure 14.

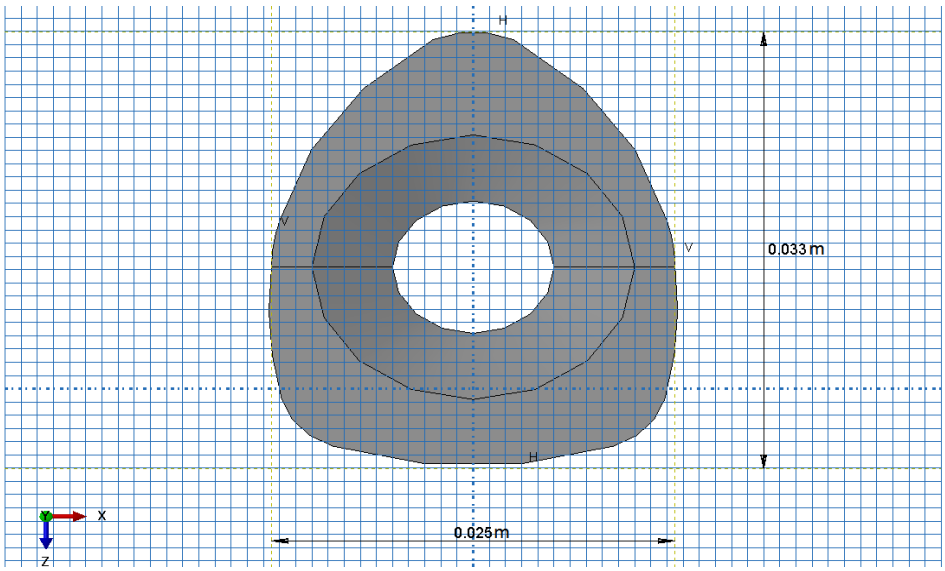

Figure 14: [Proximal cross-section of the full tibia diaphysis model]

In order to capture a more realistic cortex thickness throughout the diaphysis, the diameter of the inner hole was decreased from proximal to distal; at the proximal end, the inner diameter was 0.02m which tapered off to 0.01m at the distal end.

4.1.3 Full Diaphysis with Porosity

This same basic geometry was used to model the diaphysis with increased porosity due to osteoporotic bone loss. As bone loss occurs due to the negative remodelling balance, the porosity of the cortical bone in the diaphysis increases. Two levels of increased porosity were modelled in this study; one model representing around five per cent porosity and another model representing around 10 per cent porosity. The rough value of five per cent general porosity was represented as longitudinal canals which run though the length of the diaphysis as shown in Figure 15.

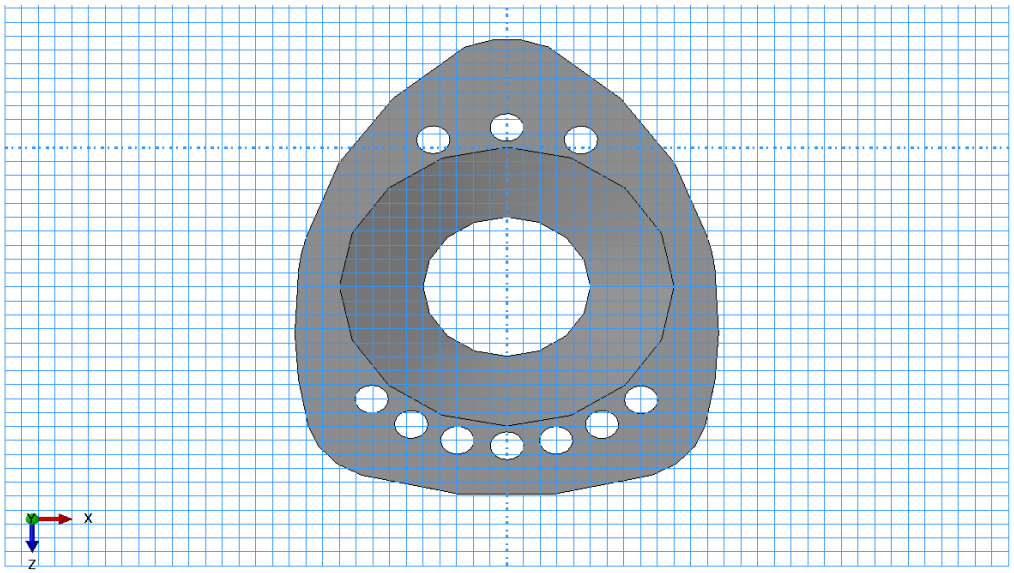

Figure 15: [Cross section of the proximal surface of the 6% porosity full diaphysis model]

Each of the small holes positioned around the circumference of the endosteal edge were 0.002m in diameter. This size for the holes was elected due to the fact that when smaller, more realistic holes were modelled the computing time was greatly increased and became unreasonable. Although the 0.002m diameter does not accurately represent the size of the pores, it gives a general idea of how the cortical bone structure will behave with an added increased bone remodelling induced porosity. The volume of the model without the models was calculate by ABAQUS ®

as $1.69 \times 10^{-4} m^3$ and to obtain this value of around five per cent porosity, ten holes of 0.002 diameter were added to give a new model volume of $1.58 \times 10^{-4} m^3$.

A second porous diaphysis model, with around ten per cent porosity was created by adding a number of extra 0.002m diameter holes were added to the model as shown in Figure 16. Again these pores ran though the length of the diaphysis.

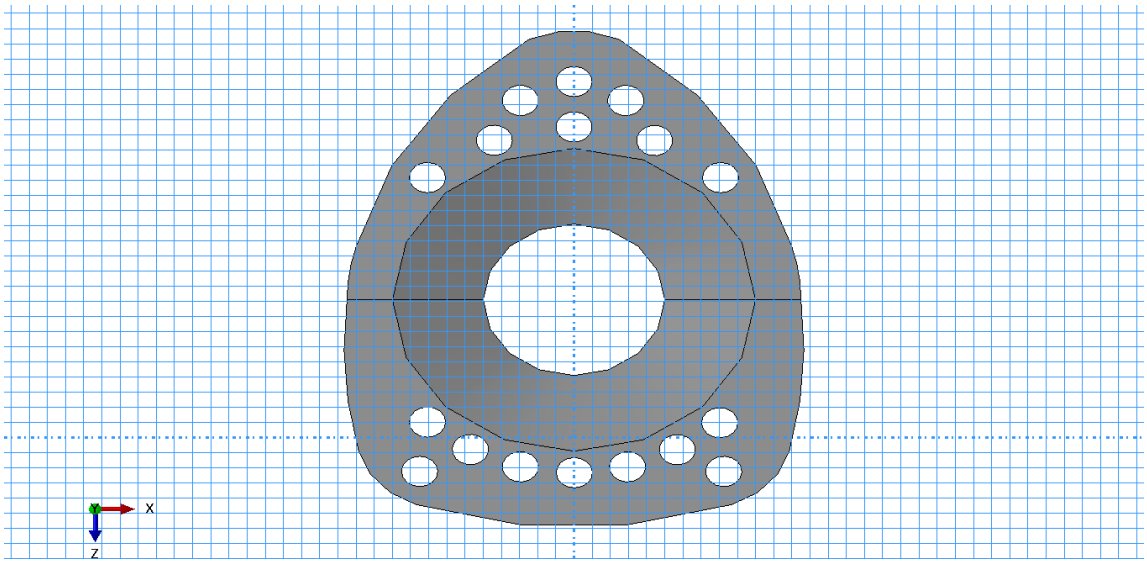

Figure 16: [Cross section of the distal surface of the 10% porosity full diaphysis model]

4.1.4 Full Diaphysis Model with Differing Density

The geometry of the tibia shaft with differing density was the same as stated for the healthy model of the full diaphysis. A common occurrence in osteoporotic bone is loss of bone density from the endosteal surface inwards resulting in a circular area of lower bone density. Due to the higher remodelling activity on the endosteal surface, there is an increased amount of remodelled bone with lower density though the length diaphysis at this area. In order for a different density to be assigned to an inner circular region, the model was partitioned as shown in Figure 17. This means that specific material properties can be assigned to the outer section and another set of material properties to the inner circular section.

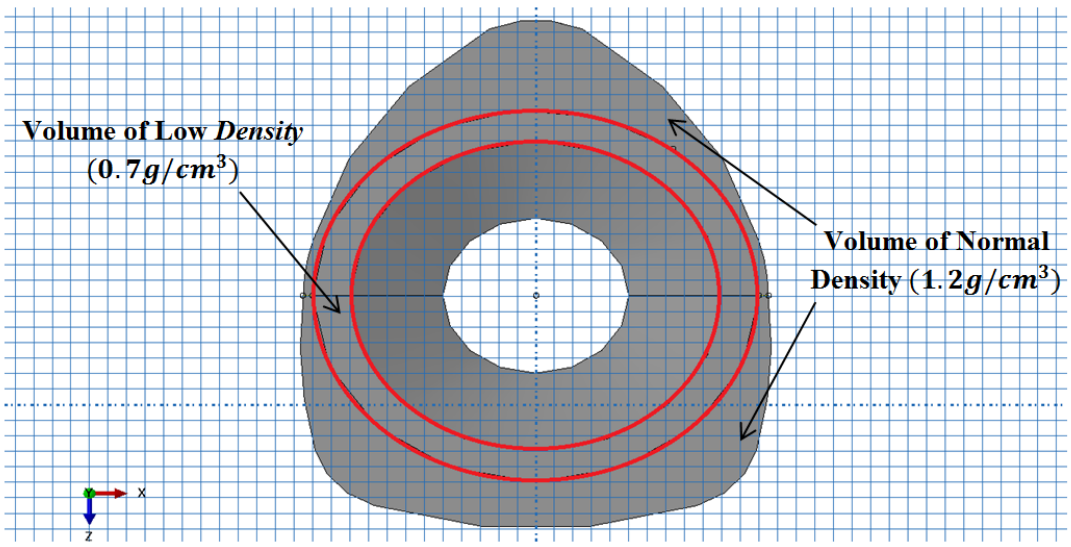

Figure 17: [Location of the partition to allow for assignment of low density cortical bone material properties to are area round the endosteal surface throughout the length of the bone]

4.2 Material Properties

As discussed in Chapter 2, cortical bone material is a complex composite material which is anisotropic and inhomogeneous by nature. The anisotropy and inhomogeneity of cortical bone material can be extremely difficult to accurately represent in a finite element model (Sharma et al., 2012). For this reason, a number of studies have modelled cortical bone as a linear elastic material (Taylor et al., 2002). However, it has been suggested that attempting to capture cortical bones anisotropic nature can lead to more accurate and realistic results (Kejak, 2001). Reilly, D and Burstein, A. (1974) proposed that cortical bone is best described as a transversely isotropic.

4.2.1 Elastic Properties

For this study transversely isotropic material properties were assigned to the bone models. The same elastic properties were assigned to all of the models. This was done by assigning five elastic constants. These elastic constants were a longitudinal and transverse Young's modulus (E_L; E_T) and shear moduli (G12; G13; G23) and a Poisson's ratio. Young's moduli values of 17.4GPa (E_L) and 14GPa (E_T) were assigned to the model to represent the longitudinal and transverse stiffness respectively (Cowin, 2001). Two shear moduli of 8.10GPa and 5.77GPa (Sharma et al., 2012) and a Poisson's ratio of 0.3 (Belenger Querol, 2006) were also used to

complete the elastic parameters of the model. The elastic material properties were assigned to the default local coordinate system within the ABAQUS ® programme. The elastic input was as follows;

Elastic Parameter	Value
E1	14GPa
E2	17.4GPa
E3	14GPa
G12	8.10GPa
G13	8.10GPa
G23	5.77GPa
NU	0.3

Table 1: [Elastic input for the bone models using the 'Engineering constants' option on ABAQUS]

*** The numbers 1, 2 and 3 represent the Y, X and Z directions respectively and NU is the symbol for the Poisson's ratio**

4.2.2 General Properties

In healthy individuals bone density is normally around $1.2 g/cm^3$ hence this value was assigned both to the full tibia shaft model and the section of the shaft models. For the area of low density discussed previously a value of $0.7 g/cm^3$ was assigned.

4.3 Mesh and Element Selection

In this study, two different types of mesh were used; a mesh of hexahedral shaped elements was assigned to the segment of the diaphysis model and tetrahedral shaped elements were used to comprise the mesh assigned to the model of the full diaphysis. The mesh was specifically chosen and altered in order to gain the most accurate results for each of the model shapes.

4.3.1 Segment of Diaphysis Model

The mesh that was assigned to this model was comprised of quadratic reduced integration continuum elements, C3D8R. The simple and uniform shape of the model allowed for these linear eight-node brick elements to be used to obtain an accurate solution within approximately five minutes computing time. A study carried out by Keyak, J. and Skinner, H. (1992) investigated the effect of element size when

constructing finite element models of bone. They observed a decrease in the stress and strain values when element sizes of 3mm and greater were used. An element size of 1mm was used in order to obtain the most accurate stress and strain values possible. The mesh used for these models is depicted in Figure 18.

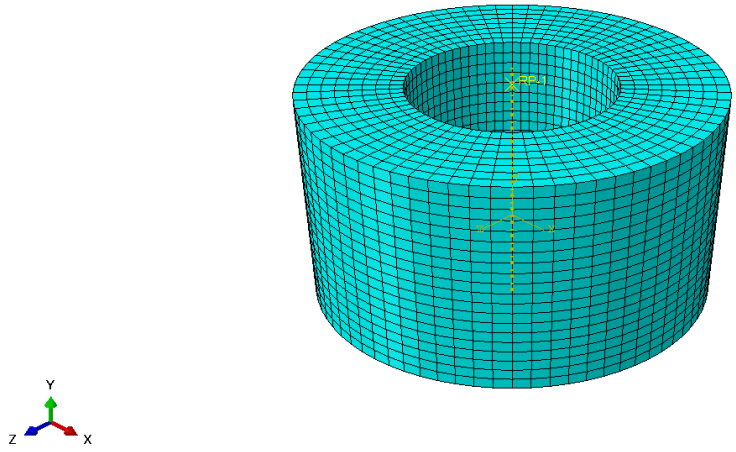

Figure 18: [Model of the cortical bone from a segment of the tibia dialysis, discretised with eight-node hexahedral continuum elements]

4.3.2 Full Diaphysis Model

Due to the more complex shape of the full diaphysis model, the quadratic reduced integration hexahedral continuum elements used previously was not appropriate. The more irregular shape of the model required that quadratic tetrahedral continuum elements, C3D10, were used. These types of element have been previously used by Gray, H. et al. (2008) in order to effectively model the human tibia bone and has been used as the element type for bone in a number of other studies and allow for both translational and rotational movement (Cheung and Zhang, 2006; Trabelsi et al., 2008; Yoshibash et al., 2007). An element size of 0.003m was assigned to the elements throughout the length of the diaphysis model and the element on the proximal surface where the highest stress concentrations were expected was assigned an element size of 0.001m. It was not practical to discretise the full model with element sizes of 0.001m as this resulted in unreasonable lengths of computing time. When simulations of this full diaphysis model discretised with 0.001m were

attempted, approximately 48 hours passed with no results. The constructed mesh shown in Figure 19 consisted of 285931 nodes and 182953 elements.

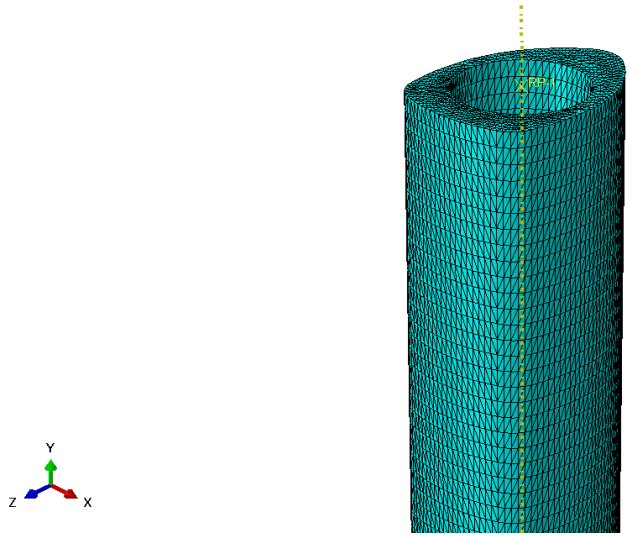

Figure 19: [model of the cortical bone of the full diaphysis, discretised with tetrahedral continuum elements]

4.4 Boundary Conditions and Application of Load

For the determination of the initial boundary conditions of the model and for the application of load, there were three sets of nodes and geometry created in order to make the process easy to carry out and replicate. Two sets of nodes were created, one set consisting of the nodes on the distal surface of the models and the other set being the nodes on the proximal surface. A set consisting of a reference point located at the centre of the inner circle was also created. The reference point was tied by kinematic coupling to the specified nodes, either on the proximal or the distal surface. This reference point was used to apply the load, as a specific magnitude of load could be applied to the reference point and it would be distributed over all of the nodes on the proximal or distal surface of the model.

4.4.1 Uniaxial Compression

A uniaxial compression testing configuration was simulated by applying specific boundary conditions to the sets that were created. Fixed displacement constraints were applied to the set of nodes on the distal surface of the model to ensure that the nodes were fully constrained in the X, Y and Z plane. The nodes on the proximal surface of the model were fixed in X and Z and left unconstrained in the Y plane.

The reference point that was used for the load application was tied to the nodes on the proximal surface and was fixed in the X and Y plane and left unconstrained in the Y plane. The nodes of these continuum elements also have rotational degrees of freedom and for this uniaxial compression test, all rotational degrees of freedom on the top and bottom surfaces were constrained so that no rotational movement of the model could occur. These boundary conditions were the initial conditions of the model prior to application of any load and allowed for the model to translate in the Y direction once the load had been applied. A pictorial representation of the uniaxial compression initial boundary conditions that were applied to the segment of diaphysis model can be seen in Figure 20.

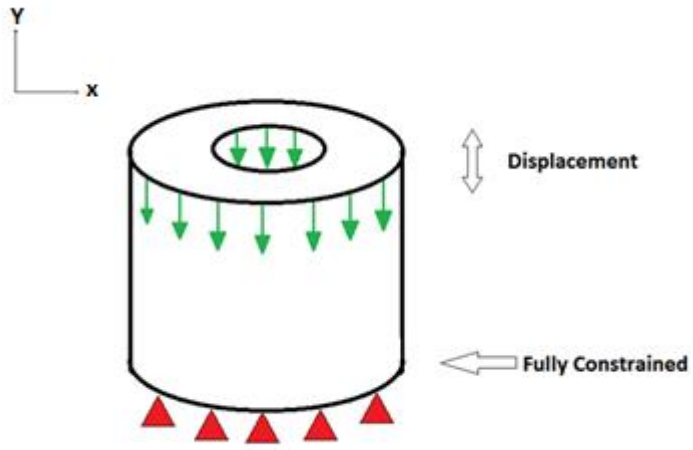

Figure 20: [Initial boundary conditions for uniaxial compression]

A compressive load of 8000N was applied to the models by creating a static general load step and entering -8000 as the load value in the Y direction.

4.4.2 Torsion

A torsional test configuration was developed by constraining the model so that the proximal end was fixed in space and the distal end could rotate as a moment was applied to it. This torsion set up was achieved by applying fixed translational and rotational constraints to the nodes on the proximal surface of the diaphysis model. These initial boundary conditions ensured that the nodes on the distal surface were

free to rotate around the long axis of the diaphysis model and the nodes on the proximal surface were fixed in space when the moment was applied. The reference node was tied to the nodes on the distal surface of the model. A moment of 70Nm acting round the y axis was applied to the reference point to simulate the replicate the torsional loading conditions of the study carried out by Gislason, M. et al., (2103).

Figure 21: [Experimental set up of a torsion test on the diaphysis of a human tibia using an Instron mechanical testing machine] [taken by Dr Caroline Newe, with permission from the Laboratory of Human Anatomy at the University of Glasgow]

Figure 21 shows the experimental torsion set up that was replicated using the finite element method in this study. The testing machine applied torque to the upper end of the bone shown while the bone was fixed at the lower end.

4.5 Analysis

The output parameters allow for the calculation of the desired vales. The history output was set to displacement and reaction force in order to calculate the stresses throughout both of the models.

4.5.1 History Output

The history output was set to measure the displacement and reaction forces of the nodes throughout the load step, allowing for the calculation of the Von Mises stresses throughout the model. This enables for the Von Mises stress values at specific points in the model to be analysed and represented graphically. Von Mises stress values are commonly used in a number of fields by engineers in order to quantify the safety of their designs. Von Mises stress values have been effectively used in previous studies to analyse the stress distribution and fracture behaviour of tibia and fibula finite element models (Wong et al., 2010). Text files of the Von Mises stress results from the models of the section of the diaphysis were obtained in order to calculate the appropriate percentages of elements over a certain stress value. This procedure was not carried out for the larger models as it was not possible to analyse the large amount of output data that was obtained with the resources available.

4.5.2 Risk of Fracture

The risk of fracture equation shown in Equation 1 previously was used to calculate the maximum risk of fracture in each of the full size diaphysis models. This was done to give an indication of what loading conditions would be likely to cause fracture in the most elements and at what locations of the models. For the compressive loading condition, an ultimate compressive strength of 161MPa was used and an ultimate strength for torsional loading of 84MPa was used to calculate the risk of fracture (Beaupied et al., 2007).

4.6 Assumptions

Several assumptions had to me made in order to construct the bone models on ABAQUS®. The general shape of the tibia diaphysis was simplified to a triangular cross section that was uniform throughout the length of the model. In reality this cross section is not a symmetrical triangular shape as modelled in this study. Also the

inner section of the models was simplified to a circular shape when it is more complex in reality.

Chapter 5 - Results

5.1 Uniaxial Compression of the Diaphysis Segment

The difference in stress distribution between the healthy and the osteoporotic segments of the diaphysis can be seen on Figures 22 and 23. Both of the models showed a similar distribution of higher stress round the circumference of the outer edge.

The maximum Von Mises stress observed in the model of healthy cortical bone loaded in uniaxial compression is 15.89MPa. As can be seen from the image in Figure 22, the elements with stress values around 15MPa are those at the outer edge of the model.

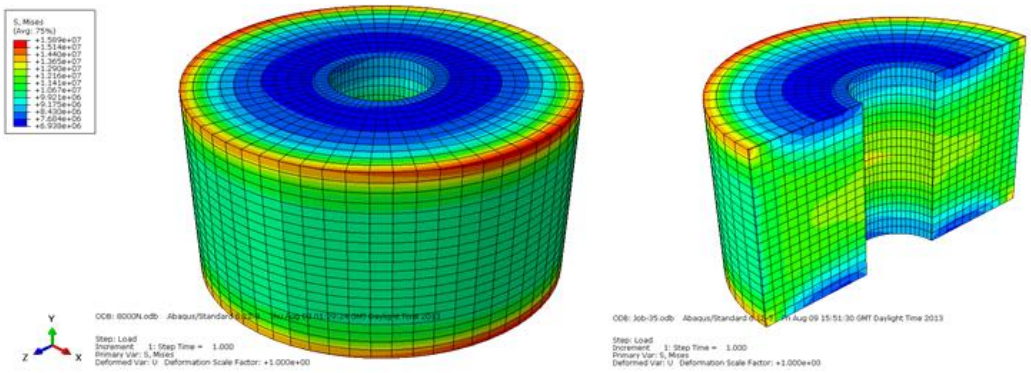

Figure 22: [Healthy segment of the diaphysis]

The maximum Von Mises stress that was calculated for the model representing osteoporotic bone loss from the endosteal surface was 19.03MPa. Again the highest stress values were located around the edge of the outer circumference. However, an area of increased stress can also be seen around the middle of the endosteal surface as shown in Figure 23.

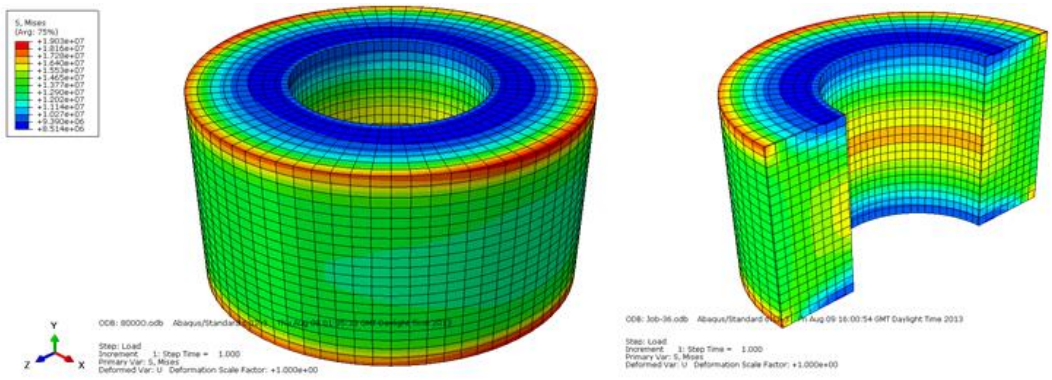

Figure 23: [Segment of the diaphysis showing osteoporotic bone loss from the endosteal surface]

Although the difference in maximum stress values in both these models appears to be fairly modest, the true effect of the endosteal bone loss can be quantified by analysing the number of elements within the models that have these high stress values. As stated earlier, the healthy diaphysis model shows a maximum Von Mises stress of 15.89MPa, however only 0.42 per cent of the elements within the model have stress values greater than 15MPa. In contrast 18 per cent of the elements within the model of the osteoporotic diaphysis have stress values above 15MPa.

5.2 Uniaxial Compression and Tension of Full Diaphysis

The results obtained from the compressive and torsional loading tests can be seen in Table 2 below;

	Uniaxial Compression		**Torsion**	
	Max Stress (MPa)	**Max RF**	**Max Stress (MPa)**	**Max RF**
Normal	30.98	0.19	46.92	0.56
Low Density	30.44	0.19	47.28	0.56
5% Porosity	32.59	0.20	56.13	0.67
10% Porosity			86.89	1.03

Table 2: [Maximum stress values and maximum risk of fracture all of the full tibia diaphysis models]

The calculation of the maximum risk fracture given in Table 2 can be seen in Appendix A.

5.2.1 Uniaxial Compression

The uniaxial compression applied to the proximal end of the diaphysis results in areas of high Von Mises stress on the outer edges of the proximal surface as can be seen in Figure 24.

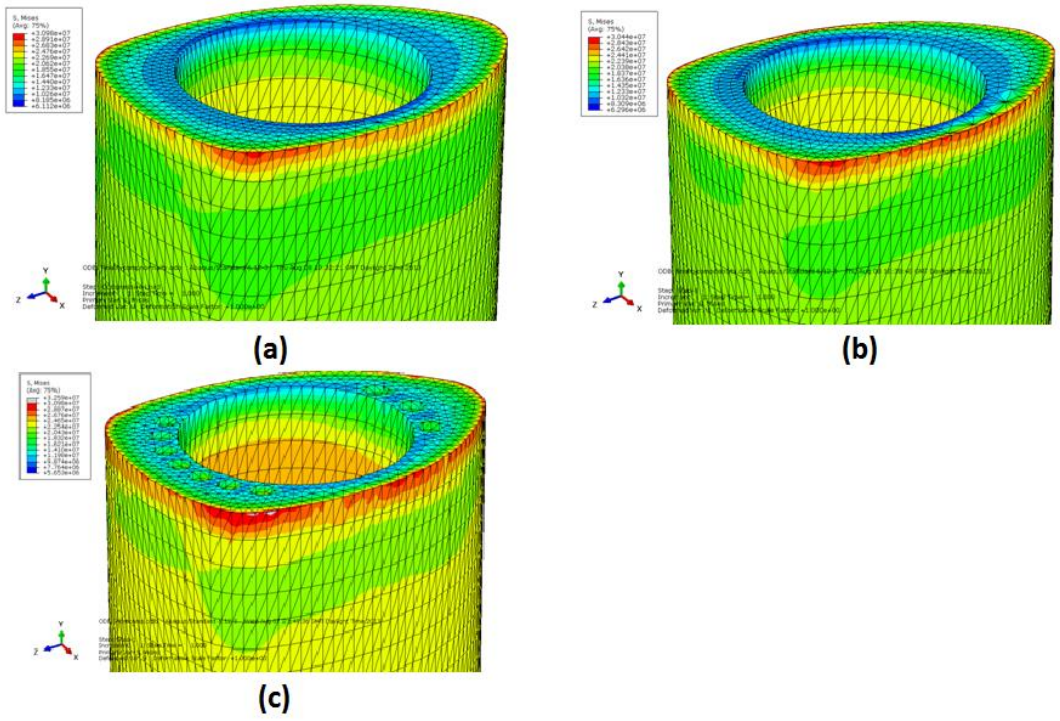

Figure 24: [Stress distribution resulting from uniaxial compression of the full diaphysis models. (a)-Healthy diaphysis; (b)-Low density diaphysis; (c) 5% porosity diaphysis

For the model of the healthy diaphysis, a maximum stress value of 30.98MPa was calculated and there were very small areas of high stress around the corners of the proximal edge observed. This distribution of high stress is slightly larger and spreads round most of the proximal edge in the model with the section of low density. For this model, the maximum stress value is around the same as was calculated for the healthy model. As can be seen from image (c) in Figure 25, the porous diaphysis models showed larger areas of high stress and had a maximum stresses of 32.59MPa.

5.2.2 Torsion

When the models of the full diaphysis were subjected to tensile loading at the distal surface, areas of high stress were observed in the proximal third of the diaphysis in each of the four models as shown in Figure 25. The stress distribution for each of these models can be seen in more detail in Appendix B.

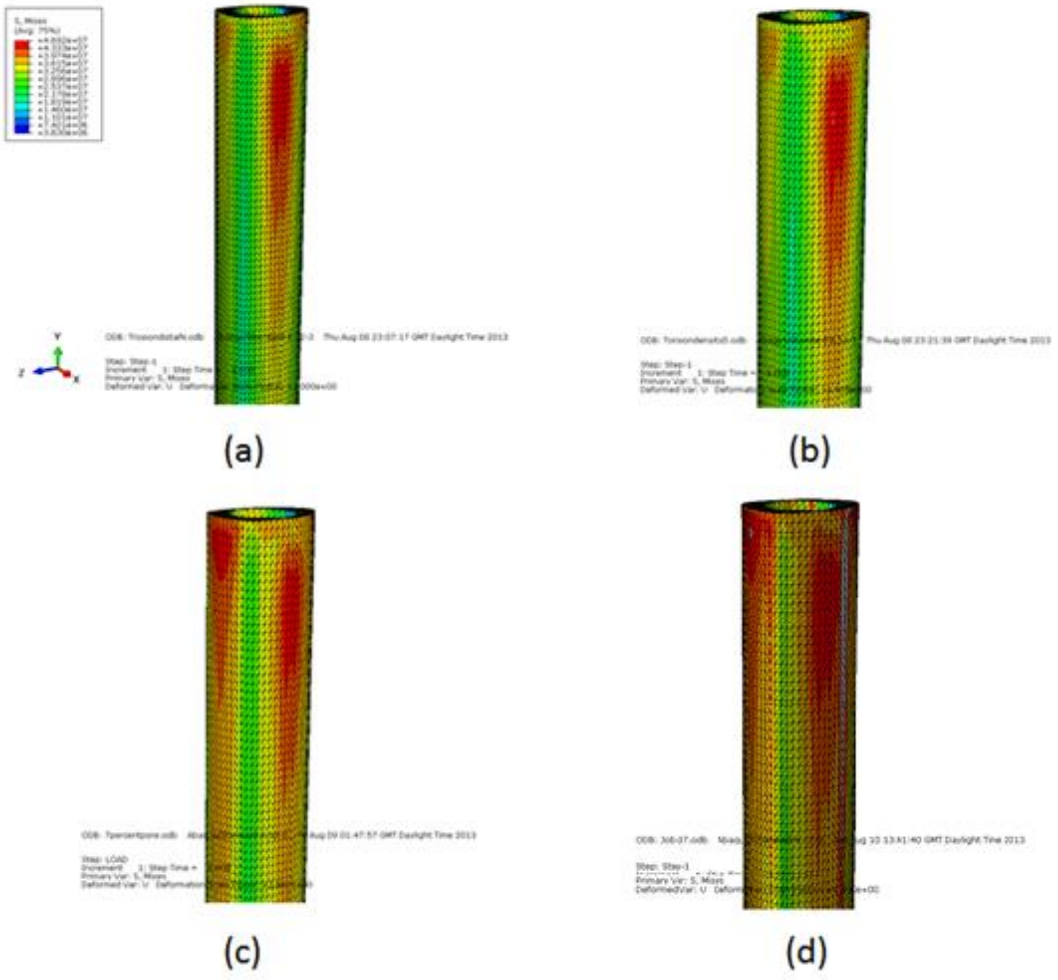

Figure 10: [Stress distribution resulting from torsional loading. (a)- Healthy diaphysis; (b)- Low density diaphysis; (c)- Diaphysis with 5% porosity; (d)- Diaphysis with 10% porosity]

*** The maximum value of $4.692\times 10^{7} Pa$ displayed on the contour is the maximim stress value for the heatlhy diaphysis model and was set as the maximum contour value for the three subsequent models to allow for a greater ease of visual inspection.**

When the healthy diaphysis model was subjected to the torsional loading, a maximum Von Mises stress value of 46.92MPa can be seen and these maximum values are located in the proximal third of the diaphysis on the medial and lateral side on the diaphysis. As can be seen in image (b) in Figure 24 there exists a similar stress distribution in response to torsional loading in the diaphysis model with a section of low density. This model has a maximum stress value of 47.28MPa.

The introduction of porosity to the model significantly increased Von Mises stress values calculated when the models were subjected to torsional loading conditions. As well as the high levels of stress seen on the medial and lateral sides of the diaphysis, there is also an area of high stress on the posterior face of the model as can be seen in images (c) and (d) in Figure 25. The model of the diaphysis with around five per cent porosity has a maximum stress value of 56.13MPa and a maximum stress of 86.89MPa was observed in the model with around ten per cent porosity.

Chapter 6- Discussion

The finite element models that have been developed in this study have allowed for comparison of fracture risk and stress distribution of osteoporotic bone to that of healthy bone. These models of the tibia diaphysis are extremely useful in clinical practise as they allow for high levels of loading to be applied in order to assess where and under what loading conditions fractures are most likely to occur in persons who have sustained significant osteoporotic bone loss. The high levels of the loading that can be applied to the computer models exceed what would be practical and possible when assessing living SCI ad osteoporotic patients. The computational models that have been developed in this study offer a fairly accurate representation of the bones geometry and the testing of the models clearly doesn't have any of the ethical and waiting time issues associated with experimental testing. This means that computational models representing osteoporotic symptoms can be developed tested and analysed with the subsequent stress results can being used to aid in patient assessment and rehabilitation.

Everyday activities subject the bones of the human skeleton to compressive, tensile and torsional forces. The everyday activities that healthy individuals perform with ease can cause fractures in people with osteoporosis. Torsional loading, and to an extent compressive loading, is more clinically relevant for SCI patients who have pronounced disuse-related bone loss. The models of the full diaphysis that were constructed in this study showed that for both healthy and osteoporotic bone, the stresses that were witnessed in torsion were significantly higher than those resulting from the compressive tests. Along with these higher stresses, the lower ultimate torsional strength of cortical bone compared to the ultimate compressive strength means that fractures induced by torsional loads are of great concern. Analysis of the loads which may cause these torsional fractures in osteoporotic bone is essential due to the prevalence of torsional fractures in SCI patients. These fractures normally occur as the SCI patient transfers from one surface to another (Gislason *et al.*, 2013). An example of this is when a SCI patient attempts to stand up in order to get out of a wheelchair and into a bed, they will push upwards while their foot remains planted

on the ground and as their lower leg rotates medio-laterally, the tibia is subjected to a torsional force. The torsional loading set up in this study mimicked this specific motion making the study loading conditions clinically relevant. The tibia diaphysis was the focus of this study due to and three symptoms of osteoporosis seen in SCI persons were modelled to allow for the results to be used for clinical assessment.

6.1 Endosteal Bone loss

As Nishiyama, K. *et al.* (2010) describes, the cortex of the tibia undergoes thinning with age and disease. As bone strength is directly related to bone mass, it is evident that this will have an adverse effect upon the bones load bearing capabilities. The afore mentioned loss of bone from the endosteal surface seen in osteoporotic persons gives rise to a significantly weaker structure, increasing the risk of fracture when performing everyday activities. The models representing a segment of the tibia diaphysis indicated that there is an increase in stress and larger area of high stress in the model representing endosteal bone loss when the same load is applied. When cortical bone is loaded in compression the maximum stresses are seen on the outer edges of the cross section (Reilly and Burstein, 1974). This pattern of stress distribution was observed in the models created in this study. As well as the expected levels of high stress on the outer edges of the cross section, uniaxial compression of the model representing endosteal loss of bone also induced a region of high stress within the bone, on the endosteal surface. The difference in percentage of high stress elements given in the results section, illustrate the greater potential for fracture in bone with increased endosteal bone loss. Although these models are only a section of the diaphysis and are fairly simple geometrical structures, they convey the general weakening effect that this bone loss has on the tibia structure.

6.2 Low Density

Rittweger, J. *et al*, (2000) reported that the mechanical properties and behaviour that make bone a mechanically sound structure are vitally dependent on its apparent density. As mentioned earlier in this study, the level of bone mineral density within the cortical bone dictates the strength and stiffness of the bone. The more geometrically realistic bone model of the tibia diaphysis developed in this study allowed for the effects of low density to be analysed. The 8000N and 70Nm that that

these models were subjected to in compression and torsion respectively, allowed for a direct comparison of results to the larger study carried out by Gislason, M. *et al.*, (2013) in which QCT derived tibia bone model of SCI persons were tested in the same loading conditions as this study. The general consensus that compressive loading is not a major cause of fracture in the tibia of SCI persons is backed up by this study Gislason, M. *et al.*, (2013). They report that in the majority of the tibia bone models for the SCI persons loaded in compression, less than one per cent of the elements have a RF value greater than one. The maximum risk fracture of the low density model constructed in this study was only 0.29, which indicates that no elements in this model have a RF greater than one. There is little difference in the maximum stress values and the RF value between the models of the healthy and low density diaphysis. However, there is a marginally larger area of high stress around the edge of the cross section in the low density model. Again, these results for uniaxial compression relate well to the larger study, as in general the RF values calculated for SCI persons were not significantly higher than those calculated for the healthy controls.

When the low density model in this model was subjected to a 70Nm torque, the maximum stress and maximum RF value was again around the same for the healthy diaphysis model. However, it should be noted that both these values were greater than those resulting from compressive loading. These results imply that fractures of the tibia are more likely to occur under torsion rather than under compression. The study by Gislason, M. *et al.*, (2013) found that in a number of SCI models there were a significant percentage of elements that had a RF greater than 1 when subjected to a torque of 70Nm. The maximum RF for the low density model of this study was only 0.56 and the area of maximal stresses was located in the proximal third as compared to the distal third as seen in the models of the larger study. These observations indicate that the simplified geometry could have been the cause for the vastly different locations of maximum stress and hence fracture location. The geometry of the models in this study is more uniform and regular in comparison to the QCT derived models which included the epiphyses and the metaphysis and have an accurate representation of the cortex thickness throughout the tibia.

6.3 Increased Porosity

Osteoporosis was first defined over a hundred years ago as bone with enhanced porosity (Ferretti et al., 2002), and although subsequent studies have furthered the osteoporosis definition there has always been a general acceptance that osteoporosis results in greater porosity of the bone. A study investigating the dependence of the elastic properties of cortical bone on porosity, Dong, N. and Guo, E. (2004) describe porosity as being one of the 'hallmarks' of osteoporosis which causes significant reduction of strength in the ling bones of the human skeleton. As the level of porosity increases, the stiffness of the cortical bone decreases (Currey, 1988). This porosity occurs as a result of the increased remodelling activity in osteoporotic bone and the tibia models representing this increased porosity developed in this study were significantly weaker and more likely to fracture as expected.

When a porosity of five per cent was added to the model of the diaphysis, an increase in maximum stress of around 10MPa and an increase in the maximum risk fracture were seen. These results give an indication of the weakening effect that increased porosity has on the bone. However, increasing the porosity level to around ten per cent results in a true representation of the damaging effects osteoporosis can have on the cortical bone. The models of the diaphysis with a porosity of around ten per cent have a maximum stress that indicates that the bone is no longer behaving elastically but has entered the plastic region. This means that a torque of 70Nm causes the osteoporotic bone to undergo irreversible deformation. This observation is in keeping with the reported lower stiffness in bones with decreasing cross-sectional area; the addition of the pores to the models decreased the cross-sectional area of the diaphysis. There is also a high likelihood that this level of porosity will result in fracture of the bone when this torsion load is applied, as there are a number of elements within the structure that have a RF greater than one. This risk of fracture result can be used clinically to ensure that patients who have a similar level of porosity are not subjected to high torsional loading conditions.

6.4 Limitations

Although these results are fairly similar to that of the study carried out by Gislason, M. *et al.,* (2013) and give a good indication of the effects these osteoporotic

symptoms have of the fracture risk of the tibia diaphysis, there are a number of limitations with the models. The shape of inner area of the diaphysis where the trabecular bone and marrow would be located was simplified to a circle when in reality the shape is less uniform and varies along the length of the diaphysis. This factor could lead to errors in the resulting stress values. With regards to the bone model representing increased porosity, the size and shape of the pores were a limitation of this study. The increased porosity of the bone was represented in the form of longitudinal canals as opposed to pockets of porosity which would be more realistic. Due to the fact that the bone models were developed using only the ABAQUS ® geometry tools, longitudinal canals where the only way to represent the significant structural porosity of the bone. Although this is a limitation, the longitudinal canals still give an idea of what effect increased bone porosity has on the load bearing strength and the fracture risk of the tibia diaphysis. It should be noted that the 8000N compressive loads that were applied are greater that what would be considered physiologically realistic, however the use of this loading value allowed for direct comparison to the results of the afore mentioned bone density study.

Chapter 7- Overall Conclusions

7.1 Brief Summary of Findings

To summarise, the greatest risk of fracture was seen when the high porosity diaphysis models were subjected to a torsional load on 70Nm. This is the only loading condition that resulted in elements with a RF value greater than one. This means that fracture is likely to occur in bone with this level of porosity and under this loading condition. The small models which represented a section of the diaphysis also indicated that bone loss from the endosteal surface produces higher strass values are a greater area of high stress. Although these models do not represent the whole tibia diaphysis they give the show that this thinning of the bone could lead to a higher risk of fracture. Modest effects were seen when the bone models were loaded in compression. As expected, the bone of osteoporotic patient is more likely to fracture when subjected to a torsional load than when compressed.

7.2 Clinical use

This study offers a valuable insight into how the diaphysis of the tibia behaves when subjected to common loading conditions. The compressive and torsional loading conditions that were modelled in this study mirror those loading conditions that are the common cause of fracture for SCI patients. The calculation of risk of fracture values for different symptoms of osteoporosis under different loading conditions allow for a quick understanding of what patient are at most risk of fracture and under what loading conditions. This means that assessment and rehabilitation planning of SCI patients can be effectively carried by relating their bone condition to one of the models developed in this study. Although the QCT derived bone models offer more accurate representation of the whole bone, these models can be used to focus solely on the fracture likelihood of the diaphysis without the lengthy scanning times that are associated with QCT scans. In the future the models in this study will be used in conjunction with QCT derived bone models in order to gain the most efficient fracture prediction possible.

Bibliography

Ashman, R. and Rho, J. 1988. Elastic modulus of trabecular bone material. *Journal of Biomechanics*, 21 (3), pp. 177-181.

Baca, V., Horak, Z., Mikulenka, P. and Dzupa, V. 2008. Comparison of an inhomogeneous orthotropic and isotropic material models used for FE analyses. *Medical Engineering & Physics*, 30 pp. 924-930.

Beaupied, H., Lespessailles, E. and Benhamou, C. 2007. Evaluation of macrostructural bone biomechanics. *Joing Bone Spine*, 74 pp. 233-239.

Burger, E., Klein-Nulend, J. and Smith, T. 2003. Strain-derived canalicular fluid flow regulates osteoclast activity in a remodelling osteon--a proposal. *Journal of Biomechanics*, 36 (10), pp. 1453-1259

Burstein, A., Reilly, D. and Frankel, V. 1973. Failure Characteristics of Bone and Bone Tissue in Perspectives in Biomedical Engineering. *University Park Press*

Burstein, A., Currey, J., Frankel, V. and Reill, D. 1972. The ultimate properties of bone tissue: The effects of yielding. *Journal of Biomechanics*, 5 (1), pp. 35-42

Carter, D. and Hayes, W. 1977. The compressive behavior of bone as a two-phase porous structure. *The Journal of Bone and Joint Surgery. American Volume.*, 59 (7), pp. 954-962.

Carter, D. 1984. Mechanical Loading Histories and Cortical Bone Remodelling. *Calcified Tissue International*, 38 pp. 19-24.

Chamay, A. 1970. Mechanical and morphological aspects of experimental overload and fatigue in bone. *Journal of Biomechanics*, 3 (3), pp. 265-270

Cheung, J. and Zhang, M. 2006. Finite Element Modeling of the Human Foot and Footwear. *ABAQUS Users' Conference,* pp. 145-159.

Choi, K., Kuhn, J., Ciarelli, M. and Goldstein, S. 1990. The elastic moduli of human subchondral, trabecular, and cortical bone tissue and the size-dependency of cortical bone modulus. *Journal of Biomechanics*, 23 (11), pp. 1103-1113

Choi, K. and Goldstein, S. 1992. A comparison of the fatigue behavior of human trabecular and cortical bone tissue. *Journal of Biomechanics*, 25 (12), pp. 1371-1381.

Clarke, B. 2008. Normal Bone Anatomy and Physiology. *Clinical Journal of the American Society of Nephrology*, 3 (3), pp. 131-139.

Consensus development conference; diagnosis, prophylaxis and treatment of osteoporosis. *American journal of medicine* , 1991,90: 107-110

Cotton, J., Zioupos, P., Winwood, K. and Taylor, M. 2003. Analysis of creep strain during tensile fatigue of cortical bone. *Journal of Biomechanics*, 36 (7), pp. 943-949.

Coupaud, S., Mclean, A. and Allan, D. 2009. Role of peripheral quantitative computed tomography in identifying disuse osteoporosis in paraplegia. *Skeletal radiology*, 38 (10), pp. 989-995.

Cowin, S. 2001. *Bone mechanics handbook*. Boca Raton, FL: CRC Press.

Currey, J. 1959. Differences in the tensile strength of bone of different histological types. *Journal of Anatomy*, 93 (1), pp. 87-95.

Currey, J. 1969. The mechanical consequences of variation in the mineral content of bone. *Journal of Biomechanics*, 21 (1), pp. 1-11.

Currey, J. 1988. The effect of porosity and mineral content on the Young's modulus of elasticity of compact bone. *Journal of Biomechanics*, 21 (2), pp. 131-139.

Depts.washington.edu. 1998. ASBMR educational materials. [online] Available at: http://depts.washington.edu/bonebio/ASBMRed/structure.html [Accessed: 17 Jul 2013].

Dempster, W. and Liddicoat, R. 1952. Compact bone as a non-isotropic material.. *The American Journal of Anatomy*, 91 (3), pp. 331-362.

Dong, N. and Guo, E. 2004. The dependence of transversely isotropic elasticity of human femoral cortical bone on porosity. *Journal of Biomechanics*, 37 (8), pp. 1281-1287.

Ebacher, V., Tang, C., Mckay, H., Oxland, T., Guy, P. and Wang, R. 2007. Strain redistribution and cracking behavior of human bone during bending. *Bone*, 40 (5), pp. 1265-1275.

Evans, F. and Vincentelli, R. 1969. Relation of Collagen Fiber Orientation to Some Mechanical Properties of Human Cortical Bone. *Journal of Biomechanics*, 2 pp. 63-71.

Evans, F. 1976. Mechanical properties and histology of cortical bone from younger and older men. *The Anatomical Record*, 185 (1), pp. 1-11.

Fan, Z., Swadener, J., Rho, J., Roy, M. and Pharr, G. 2002. Anisotropic properties of human tibial cortical bone as measured by nanoindentation. *Journal of Orthopaedic Research*, 20 (4), pp. 806-810.

Ferretti JL, Cointry GR, Capozza RF andFrost HM (2003) Bone mass, bone strength, muscle bone interactions, osteopenias and osteoporoses. *Mechanism of Ageing and Development*, 124(3): 269-279.

Frost, H. 1969. Tetracycline-based histological analysis of bone remodelling. *Calcified Tissue Research*, 3 (3), pp. 211-237.

Gislason M, Coupaud S, Sasagawa K, Tanabe Y, Purcell M, Allan DB, Tanner KE 2013 "Prediction of risk of fracture in the tibia due to altered bone mineral distribution resulting from disuse: a finite element study" Proc IMechE Part H: J Eng Med (in prep.)

Goldstein, S., Wilson, D., Sonstegard, D. and Matthews, L. 1983. The mechanical properties of human tibia trabecular bone as a function of metaphyseal location. *Journal of Biomechanics*, 16 (12), pp. 965-969.

Gray, H., Taddei, F., Zavatsky, A., Cristofolini, L. and Gill, H. 2008. Experimental validation of a finite element model of a human cadaveric tibia. *Journal of Biomechanical Engineering*, 130 (3)

Han, Z., Palnitkar, S., Rao, D., Nelson, D. and Parfitt, A. 1997. Effect of ethnicity and age or menopause on the structure and geometry of iliac bone. *Journal of Bone and Mineral Research*, 11 (12), pp. 1967-1975.

Hill, P. and Orth, M. 1998. Bone Remodelling. *British Journal of Orthodontics*, 25 pp. 101-107.

Keaveny, T. and Hayes, W. 1993. A 20-year perspective on the mechanical properties of trabecular bone. *Journal of Biomedical Engineering*, 115 (4B), pp. 534-542

Keyak, J. and Skinner, H. 1992. Three-dimensional finite element modelling of bone: effects of element size. *Journal of Biomedical Engineering*, 14 pp. 483-489.

KO. R.: The Tension Test Upon the Compact Substance of the Long Bones of Human Extremities. J. Kyoto Pref. *Med. Univ*., 53: 503-525. 1953

Lakes, R. and Saha, S. 1979. Cement Line Motion in Bone. *Science*, 204 pp. 501-503.

Lane, N. 2006. Epidemiology, etiology, and diagnosis of osteoporosis. *American Journal of Obstetrics and Gynecology*, 194 pp. S3-11.

Lang, S. 1970. Ultrasonic Method for Measuring Elastic Coefficients of Bone and Results on Fresh and Dried Bovine Bones. *Transactions on Bio-medical Engineering*, 17 (2), pp. 101-105.

Linde, F., Norgaard, P., Hvid, I., Odgaard, A. and Soballe, K. 1991. Mechanical properties of trabecular bone. Dependency on strain rate. *Journal of Biomechanics*, 24 (9), pp. 803-809.

Majda, P. and Skrodzewicz, J. 2009. A modified creep model of epoxy adhesive at ambient temperature. *International Journal of Adhesion and Adhesives*, 29 (4).

Mcclung, M. 2005. The Relationship between Bone Mineral Density and Fracture Risk. *Current Osteoporosis Reports*, 3 (2), pp. 57-63.

McElhaney, Jh and Byarse. 1965 Dynamic Response of Biological Materials. ASME 65

Mellon, S. and Tanner, K. 2012. Bone and its adaptation to mechanical loading: a review. *International Materials Reviews*, 57 (5), pp. 235-255.

Mercer, C., He, M., Wang, R. and Evans, A. 2006. Mechanisms governing the inelastic deformation of cortical bone and application to trabecular bone. *Acta Biomaterialia*, 2 (1), pp. 59-68.

Mosekilde, L. and Danielsen, C. 1987. Biomechanical competence of vertebral trabecular bone in relation to ash density and age in normal individuals. *Bone*, 8 (2), pp. 79-85.

Nalla, R., Kinney, J. and Ritchie, R. 2003. Mechanistic fracture criteria for the failure of human cortical bone. *Nature Materials*, 2 (3), pp. 164-168.

Nishiyama, K., Macdonald, H., Buie, H., Hanley, D. and Boyd, S. 2010. Postmenopausal Women With Osteopenia Have Higher Cortical Porosity and Thinner Cortices at the Distal Radius and Tibia Than Women With Normal aBMD: An In Vivo HR-pQCT Study. *Journal of Bone and Mineral Research*, 25 (4), pp. 882-890.

Peng, L., Bai, J., Zeng, X. and Zhou, Y. 2006. Comparison of isotropic and orthotropic material property assignments on femoral finite element models under two loading conditions. Medical Engineering & Physics, 28 (3), pp. 227-233.

Piekarski, K. 1970. Fracture of Bone. Journal of Applied Physics, 41 (1), pp. 215-224

Pidaparti, R. and Burr, D. 1992. Collagen fiber orientation and geometry effects on the mechanical properties of secondary osteons. *Journal of Biomechanics*, 25 (8), pp. 869-880.

Reilly, D. and Burstein, A. 1974. The mechanical properties of cortical bone- A Review. *The Journal of Bone and Joint Surgery*, 56 (5), pp. 1001-1022.

Rho, J., Ashman, R. and Turnell, C. 1993. Young's modulus of trabecular and cortical bone material: Ultrasonic and microtensile measurements. *Journal of Biomechanics*, 26 (2), pp. 111-119.

Rho, J., Kuhn-Spearing, L. and Zioupos, P. 1998. Mechanical properties and the hierarchical structure of bone. *Medical Engineering & Physics*, 20 (2), pp. 92-102.

Ritchie, R., Kinney, J., Kruzic, J. and Nalla, R. 2006. Cortical Bone Fracture. Wiley Encyclopedia of *Biomedical Engineering*, pp. 1-16.

Rittweger, J., Beller, G., Ehriq, J., Jung, C., Koch, U., Ramolla, J., Schmidt, F., Newwit, D., Majumdar, S., Schiessl, H. and Felsenberg, D. 2000. Bone-muscle strength indices for the human lower leg. *Bone*, 27 (2), pp. 319-326.

Roodman, G. 1999. Cell biology of the osteoclast. *Experimental Hematology*, 27 (8), pp. 1229-1241.

Sasaki, A., Nakayama, Y., Yoshikawa, M. and Enyo, A. 1993. Stress relaxation function of bone and bone collagen. *Journal of Biomechanics*, 26 (12), pp. 1369-1376.

Schaffler, M. and Burr, D. 1988. Stiffness of compact bone: Effects of porosity and density. *Journal of Biomechanics*, 21 (1), pp. 13-16.

Schriefer, J., Warden, S., Saxon, L., Robling, A. and Turner, C. 2005. Cellular accommodation and the response of bone to mechanical loading. *Journal of Biomechanics*, 38 (9), pp. 1838-1845.

Seeman, E. and Delmas, P. 2006. Bone Quality — The Material and Structural Basis of Bone Strength and Fragility. *The New england Journal of Medicine*, 26 (1), pp. 2250-2261.

Sharma, N., Sehgal, D., Pandey, R. and Pal, R. 2012. Finite Element Simulation of Cortical Bone under Different Loading and Anisotropic Yielding Situations.

Proceedings of the World Congress on Engineering and Computer Science. October 24-26, 2012, San Francisco, USA, 2.

Silver, I., Murrills, R. and Etherington, D. 1988. Microelectrode studies on the acid microenvironment beneath adherent macrophages and osteoclasts. *Experimental Cell Research*, 175 (2), pp. 266-276.

Thompson, D. 1942. 'On growth and form'. New York: *Cambridge University Press*.

Townsend, P., Rose, R. and Radin, E. 1975. Buckling studies of single human trabeculae. *Journal of Biomechanics*, 8 (3-4), pp. 199-200.

Torgerson D, Iglesias C and Reid DM. 2001 The Effective Management of Osteoporosis. In: The economics of fracture prevention p. 111-121.

Toshiya, I., Yasuyuki, M., Sasaki, S. and Mitsuo, N. 2004. Anisotropic viscoelastic properties of cortical bone. *Journal of Biomechanics*, 37 pp. 1433-1437.

Trabelsi, N., Yoshibash, Z. and Milgrom, C. 2008. Validation of subject-specific automated p-FE analysis of the proximal. *Journal of Biomechanics*, 42 (3), pp. 234-241.

Wang, X., Masilamani, N., Mabrey, J., Alder, M. and Agrawal, C. 1998. Changes in the Fracture Toughness of Bone May Not Be Reflected in Its Mineral Density, Porosity, and Tensile Properties. *Bone*, 23 (1), pp. 67-72.

World health Organisation (2004). Who Scientific Group On The Assessment Of Osteoporosis At Primary Health Care Level. Brussels: *WHO Press*

Wolff, J.: 'Das Gesetz der Transformation der Knochen'; 1891, Berlin, Springer-Verlag

Wong C., Mikkelsen P., Hansen L., Darvann T., Gebuhr P., 2010. Finite element analysis of tibia fractures. *Danish Medical Bulletin*, 57: 1-4

Yosibash, Z., Trabelsi, N. and Milgrom, C. 2007. Reliable simulations of the human proximal femur by high-order finite element analysis validated by experimental observations. *Journal of Biomechanics*, 40 pp. 3688-3699.

Zebaze, R., Ghasem-Zadeh, A., Bohte, A., Iuliano-Burns, S., Mirams, M., Price, R., Mackie, E. and Seeman, E. 2010. Intracortical remodelling and porosity in the distal radius and post-mortem femurs of women: a cross-sectional study. *Lancet*, 15 (375), pp. 1729-1736.

Appendix A

Risk of fracture calculations for the uniaxial compression tests;

$$RF = \frac{\sigma_{vm}}{\sigma_{UTS}} = \frac{30.98}{161.8} = 0.19 \quad (3)$$

$$RF = \frac{\sigma_{vm}}{\sigma_{UTS}} = \frac{30.44}{161.8} = 0.19 \quad (4)$$

$$RF = \frac{\sigma_{vm}}{\sigma_{UTS}} = \frac{32.59}{161.8} = 0.20 \quad (5)$$

Risk of fracture calculations for the torsion tests;

$$RF = \frac{\sigma_{vm}}{\sigma_{UTS}} = \frac{46.92}{84} = 0.56 \quad (6)$$

$$RF = \frac{\sigma_{vm}}{\sigma_{UTS}} = \frac{47.28}{84} = 0.56 \quad (7)$$

$$RF = \frac{\sigma_{vm}}{\sigma_{UTS}} = \frac{56.13}{84} = 0.67 \quad (8)$$

$$RF = \frac{\sigma_{vm}}{\sigma_{UTS}} = \frac{86.89}{84} = 1.03 \quad (9)$$

Appendix B : Full size Model Images

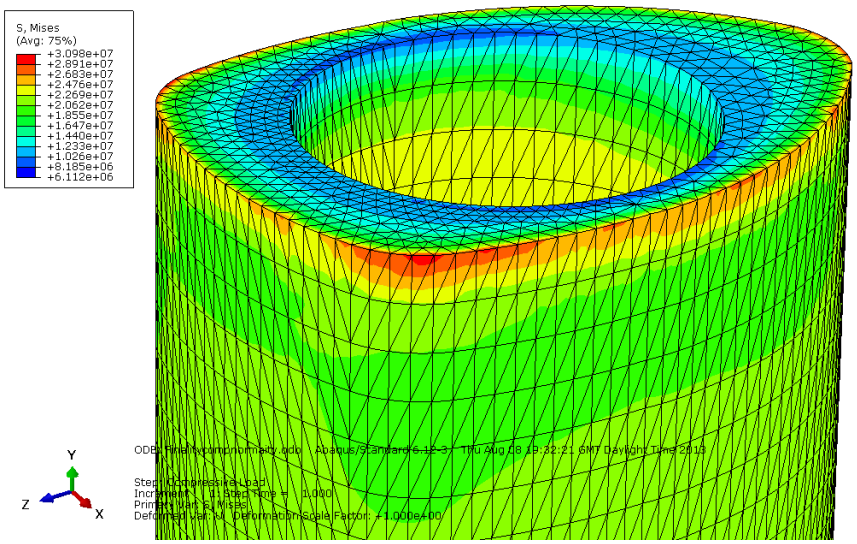

Figure 11: [Compression of healthy tibia diaphysis]

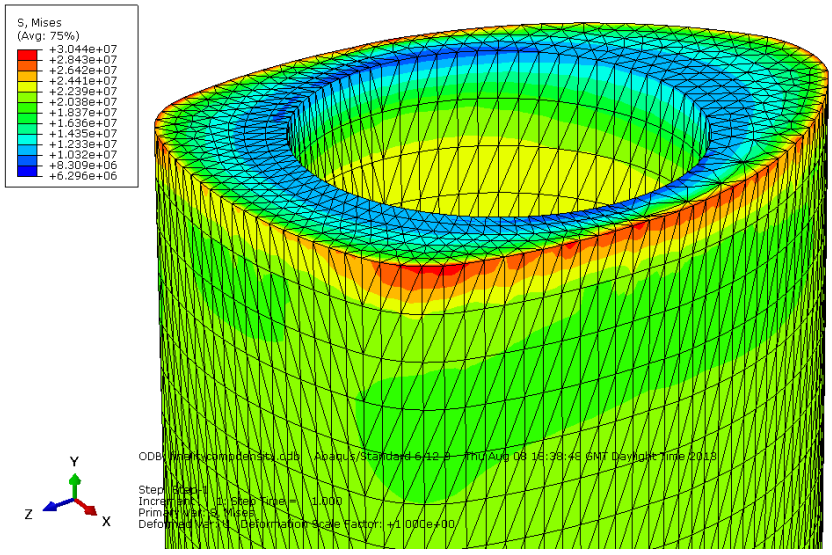

Figure 12:[Compression of low density tibia diaphysis]

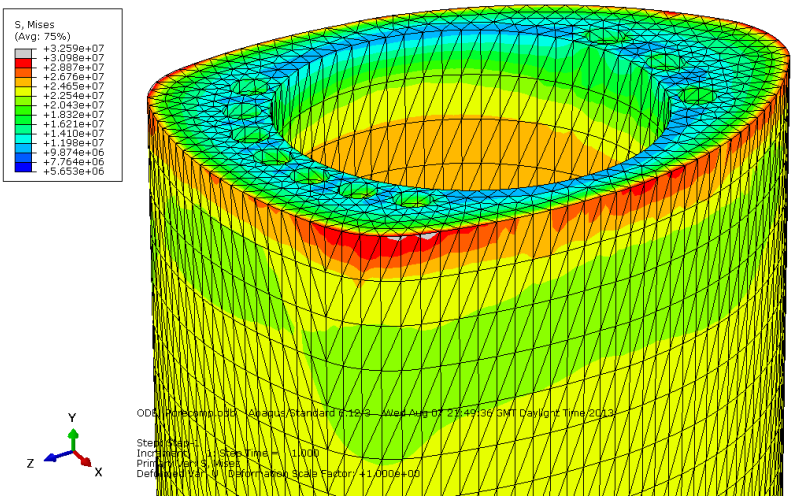

Figure 13: [Compression of 5% porosity tibiadiaphysis]

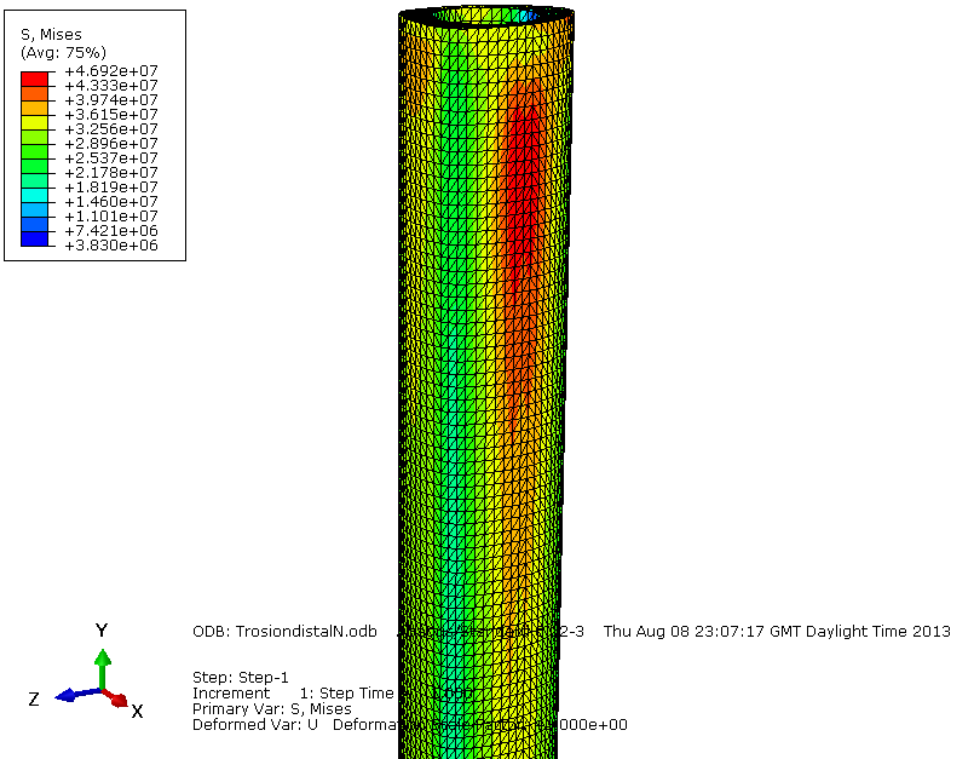

Figure 14:[Torsion of healthy tibia diaphysis]

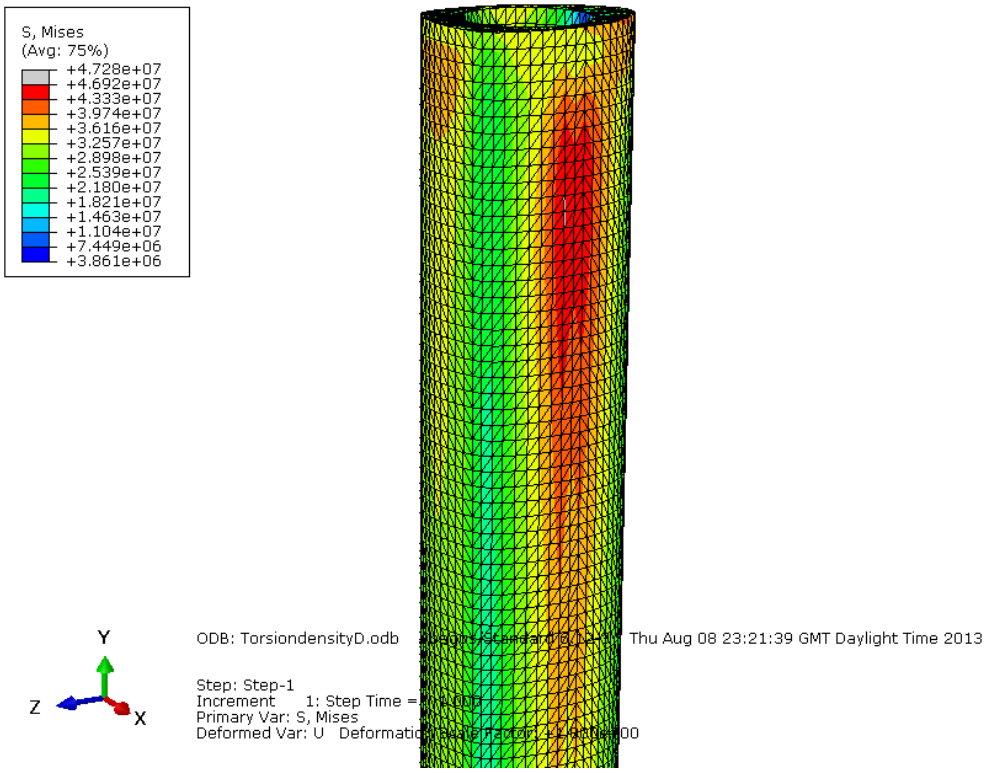

Figure 15: [Torsion of low density tibia diaphysis model]

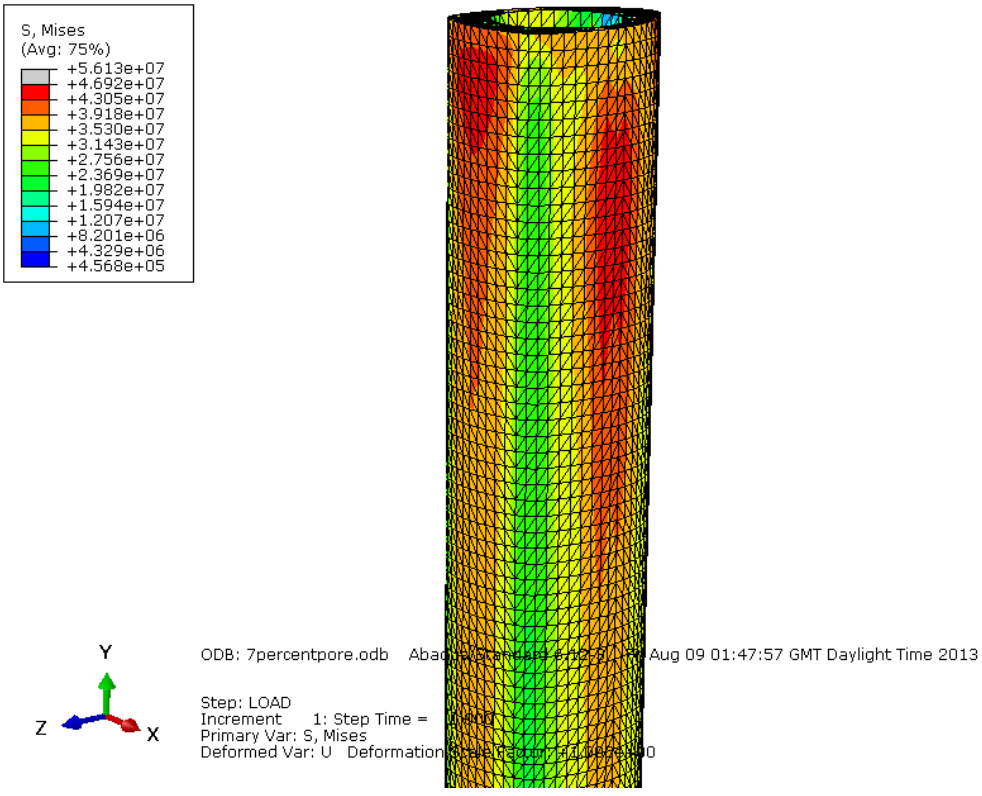

Figure 16: [Torsion of 5% porosity tibia diaphysis]

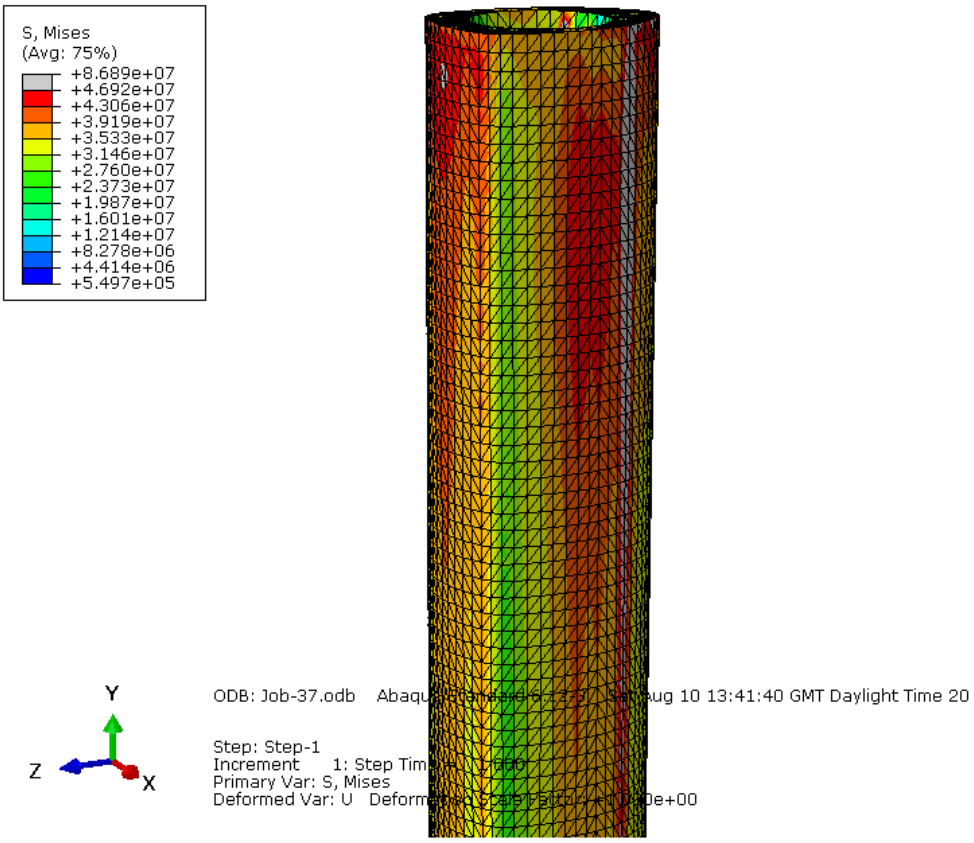

Figure 17: [Torsion of 10% tibia diaphysis model]